I&EC research
Industrial & Engineering Chemistry Research
pubs.acs.org/IECR
Article

Investigation of the Mechanisms and Kinetics of DBU-Catalyzed PLGA Copolymerization via a Full-Scale Population Balance Analysis

Samruddhi Patil, Jin Yoo, and You-Yeon Won*

Cite This: *Ind. Eng. Chem. Res.* 2021, 60, 14685−14700
Read Online

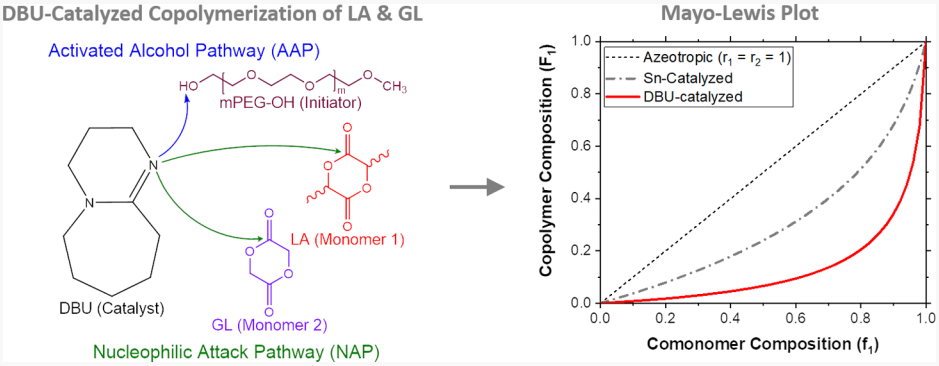

ABSTRACT: The cyclic organic amidine catalyst, 1,8-diazabicyclo[5.4.0]undec-7-ene (DBU), is gaining popularity for its use in the synthesis of biodegradable aliphatic polyesters, such as poly(lactic-*co*-glycolic acid) (PLGA). PLGA is one of the most successful polymeric drug delivery materials in the pharmaceutical industry. Currently, commercial PLGA materials are produced via ring-opening copolymerization of lactide and glycolide under the influence of metal catalysts such as tin octoate, and this chemistry has been extensively studied. However, not much is known yet about the details of the newer, DBU-catalyzed PLGA polymerization reactions. The present study is intended to address this gap. For this investigation, a full-scale kinetic population balance model was developed that takes into account all possible reactions of the copolymerization, including initiation via activated alcohol and nucleophilic attack pathways, self- and cross-propagation, combination via inter- and intrachain acylation, and DBU deactivation. Predictions of this model in terms of copolymerization rates, repeat unit sequence length distributions in PLGA products, etc., were compared with experimental data available in the literature. This analysis led to the determination of the values of 14 different reaction rate constants; nine of them were previously unknown. As illustrated in the Mayo−Lewis plot presented in the main text, the most striking finding of this study is the 3-orders-of-magnitude difference in the reactivity ratio between the two monomers, lactide (LA, monomer 1) vs glycolide (GL, monomer 2), that is, r_1 ($\equiv k^1_{p(1,1)}/k^1_{p(1,2)}$) = 3.37 × 10^{-2} and r_2 ($\equiv k^1_{p(2,2)}/k^1_{p(2,1)}$) = 13.6, in this DBU-catalyzed process; this result is in contrast to what has previously been reported for tin-catalyzed PLGA polymerization reactions (r_1 = 0.20 and r_2 = 2.8). An important implication of this result is that it is practically impossible to produce DBU-catalyzed PLGA copolymers with uniform monomer sequence distributions using an ordinary batch reaction process. We also demonstrate that the kinetic model can be used to design nonconventional, semibatch copolymerization reactors for producing monomer sequence-controlled, "uniform PLGA" products, which have constant monomer sequence characteristics along the chain. Further experimental study is warranted to demonstrate the implementation of the semibatch strategy developed using the kinetic model.

1. INTRODUCTION

Aliphatic polyesters, such as poly(lactic acid) (PLA) and poly(lactic-*co*-glycolic acid) (PLGA), are very useful for drug delivery.[1,2] There are a few commercialized drug products that are based on PLA; examples include Atridox (in situ gels) and Genexol-PM (long circulating micelles).[3−5] PLGA is even more popular; there are more than 20 FDA-approved drug products that use PLGA as an excipient,[6,7] including Lupron Depot, Eligard, Vivitrol, and Trelstar.[3−5,8−10] The reason for PLGA's popularity is its versatility. There are multiple molecular parameters that can be used to tailor the drug release properties of PLGA materials; those parameters are molecular weight, copolymer composition (lactide-(LA):glycolide(GL) ratio), end functionality (−OH vs −COOH), architecture (linear, branched vs cross-linked), and stereochemistry (D- vs L-LA).[11,12] It is only within the last

Received: August 1, 2021
Revised: September 17, 2021
Accepted: September 22, 2021
Published: October 5, 2021

https://doi.org/10.1021/acs.iecr.1c03096
Ind. Eng. Chem. Res. 2021, 60, 14685−14700

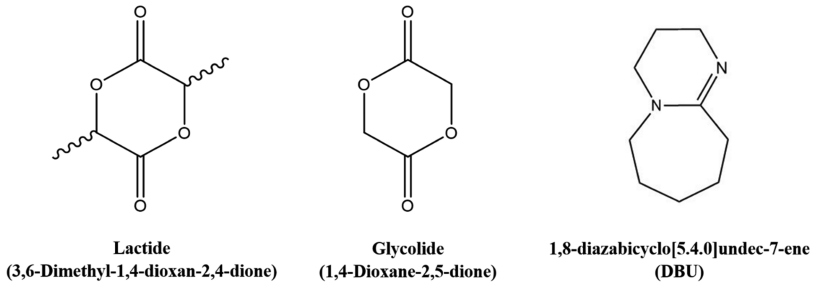

Figure 1. Chemical structures of lactide (LA), glycolide (GL), and 1,8-diazabicyclo[5.4.0]undec-7-ene (DBU).

decade or so that monomer sequence length (distribution) has also been demonstrated as a factor that influences the degradation and drug release properties of PLGA.[13−16] It has been shown that a strictly alternating copolymer of LA and GL exhibits a much slower degradation than ordinary PLGA;[15] such a property might be beneficial for certain applications. This inspires a question of whether the implementation of monomer sequence control only at the *statistical* level (not at the *deterministic* level of resolution, as demonstrated with strictly alternating PLGA) would also produce useful properties for PLGA.

The most common method of synthesizing PLGA is via ring-opening copolymerization of LA and GL (Figure 1) with an alcohol initiator in the presence of a metal catalyst. Metal catalysts, such as tin(II) 2-ethylhexanoate (stannous octoate),[17] tin(II)[17]/zinc[18]/aluminum[19] alkoxides, amino-calcium compounds,[20] and rare earth metal complexes,[21] enable the production of high-molecular-weight (MW) PLGA polymers (MW $\gtrsim$ 10 kDa) with reasonable polydispersity indices ($\approx$1.5) via a living-like polymerization mechanism (called coordination-insertion).[22−24] These reactions are typically conducted in batch reactors by introducing the two monomers, LA and GL, into the reactor at the beginning of the polymerization process. LA (monomer 1) and GL (monomer 2) have very disparate reactivities; the reactivity ratios are known to be r_1 = 0.2 and r_2 = 2.8 for the tin-catalyzed copolymerization at 200 °C.[25] Therefore, the conventional batch copolymerization process produces a *gradient* copolymer of LA and GL ("gradient PLGA") having a monomer composition varying along the chain from mostly GL at one end to mostly LA at the other (Figure 2); all commercial PLGA products are gradient PLGA materials. Although this issue has not been investigated previously, a severe gradient in composition will exacerbate the problem of poor solubility of PLGA (particularly those with LA:GL < 1) in solvents because long GL sequences are not normally soluble in ordinary hydrocarbon/halide solvents.[26,27]

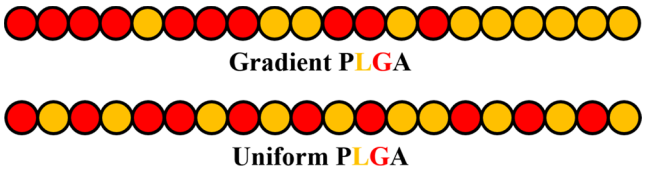

Figure 2. Cartoon describing the difference in statistical monomer sequence distribution between "gradient PLGA" and "uniform PLGA". Conventional batch copolymerization reactions produce non-sequence-controlled "gradient PLGA" copolymers because of the disparate reactivities of lactide (LA) and glycolide (GL) monomers toward polymerization. Nongradient, statistically monomer sequence-controlled "uniform PLGA" materials can be synthesized by, for instance, semibatch processes. Quantitative understanding of the mechanisms and kinetics of all component reactions is required to develop new nonbatch copolymerization processes for producing "uniform PLGA" products.

Organic catalysts have been explored as alternatives to metal catalysts for the ring-opening polymerization of cyclic esters (such as LA); seminal work is due to Waymouth, Hedrick, and co-workers,[28] and examples of such organic catalysts include various amidines (e.g., 1,8-diazabicyclo[5.4.0]undec-7-ene (DBU),[28] 1,5-diazabicyclo[4.3.0]non-5-ene (DBN)),[28,29] guanidines (e.g., 1,5,7-triazabicyclo[4.4.0]dec-5-ene (TBD),[28] *N*-methyl-1,5,7-tri-azabicyclododecene (MTBD)),[28,30] aminopyridines (e.g., 4-(dimethylamino)pyridine (DMAP)),[31] thioureas (thioimidates),[32] and *N*-heterocyclic carbenes.[29,31] Each chemistry comes with both advantages and disadvantages in terms of polymerization time, product polydispersity, etc. However, the basic chemical mechanisms are more or less similar for all of these catalysts (i.e., OH activation for nucleophilic monomer substitution and/or direct initiation via nucleophilic monomer activation). DBU was chosen for this study because it is the most studied compound in this organic catalyst class[33] and also it is the only organic catalyst that has been demonstrated for the synthesis of both LA[34] and GL.[35] Unlike tin catalysts, DBU enables the polymerization of LA and GL at room temperature and is thus capable of producing polymers with much narrower distributions of MWs (polydispersity indices on the order of ~1.1) due to the absence of transesterification side reactions.[24] DBU also completely eliminates metal contamination of the polymer product, which is especially desirable for biomedical applications.[36] However, the downside of using DBU is, as discussed in our previous publication,[37] the complexity of the reaction mechanisms involved in this chemistry. Key steps of the DBU-catalyzed LA polymerization process include initiation via activated alcohol[28] and nucleophilic attack[38] pathways, self- and cross-propagation, combination via inter- and intrachain acylation,[39] and DBU deactivation.[37] A similar set of reactions are also expected for GL.[35]

Not many attempts have been reported to copolymerize LA and GL using DBU as the catalyst. As mentioned above, the difficulty lies in the fact that, because of the significantly higher reactivity of GL compared with that of LA,[25] precipitation of the growing PLGA chains is highly possible when a batch reaction is used. This problem can be avoided through the use of a semibatch copolymerization process in which the more reactive species (GL) is continuously added to compensate for its faster consumption; the general concept has been around in the polymer reaction engineering field for some time.[40,41] Qian et al. have demonstrated that the addition of GL at a constant rate gives a quantitative yield of a PLGA having a target MW

https://doi.org/10.1021/acs.iecr.1c03096
Ind. Eng. Chem. Res. 2021, 60, 14685−14700

and composition, offering an improved method for the DBU-catalyzed copolymerization of LA and GL.[42] Designing more sophisticated semibatch PLGA polymerization processes requires precise determination of reaction parameters, which, in turn, requires a high level of resolution on the mechanisms involved and accurate estimates of the kinetic parameters. Addressing this need (i.e., elucidating the mechanisms and kinetics of DBU-catalyzed PLGA copolymerization reactions) is the goal of the present study. As published in Sherck et al.,[37] our laboratory has previously made significant progress in developing a quantitative, mechanistic understanding of the DBU-catalyzed polymerization of LA. In the present study, we hypothesize that the mechanisms for the polymerization of LA by DBU can be generalized to that of GL. Based on this assumption, we derive the kinetic balance equations describing the populations of all species involved in the LA and GL copolymerization reactions. These mechanistic equations are parameterized with data from kinetic experiments; by fitting analysis, rate constants are determined for all reactions involved (including initiation via activated alcohol and nucleophilic attack pathways, self- and cross-propagation, combination via inter- and intrachain acylation, and DBU deactivation). The reasonableness of the rate constants thus obtained supports the validity of the mechanistic model. Finally, it is also demonstrated that this kinetic model can be used for designing copolymerization reactions to produce nongradient, statistically monomer sequence-controlled, "uniform PLGA" products (Figure 2).

2. KINETIC MODELING

In the present study, we use the terminal model in which the rate of reaction with the given type of monomer depends only on the identity of the last monomer of the growing chain.[43] This terminal model is known to fail for some combinations of vinyl monomers, such as styrene + maleic anhydride[44,45] and styrene + acrylonitrile.[46] However, we believe that the terminal model is an appropriate model for the LA + GL system because each LA or GL monomer contains six carbon and oxygen atoms that are incorporated into the backbone of the chain and therefore the effect of penultimate monomers on the rate of propagation can be safely neglected. Within this terminal model, kinetic equations were derived for the first three moments of chain length distribution to describe the time evolution of all species involved in the DBU-catalyzed copolymerization of LA and GL; the equations are summarized in Sections S1−S5 of the Supporting Information (SI). With known initial conditions, the kinetic equations (48 stiff, first-order, ordinary differential equations, listed in Section S5 of the SI) were numerically solved using MATLAB's ode15s solver, which is a variable-step variable-order solver based on backward difference formulae of orders 1−5. In the present study, kinetic modeling was used for two purposes. First, the kinetic equations were fit to experimental data to estimate rate constants for all reactions involved in the DBU-catalyzed copolymerization of LA and GL. Second, using these rate constants, a semibatch operation strategy was designed for the production of a sequence-controlled PLGA copolymer.

Copolymerization rate constants were estimated in two steps. First, conversion data for LA (monomer 1) and GL (monomer 2) homopolymerization processes were fit with the kinetic model to determine homopolymerization rate constants, including the homopropagation rate constants, $k^1_{p(1,1)}$ and $k^1_{p(2,2)}$ (see Figure 6 and also Sections S1−S5 of the SI for the definitions of the rate constant notations). Next, repeat unit (lactate and glycolate) sequence lengths for PLGA copolymers produced by semibatch copolymerization processes operated at constant rates of GL addition were again fit with the kinetic model using copolymerization rate constants, including the cross-propagation rate constants, $k^1_{p(1,2)}$ and $k^1_{p(2,1)}$, as fitting parameters. Experimental data used in these analyses were primarily taken from Qian et al.[42] From these propagation rate constants, the reactivity ratios for LA and GL, i.e., $r_1 \equiv k^1_{p(1,1)}/k^1_{p(1,2)}$ and $r_2 \equiv k^1_{p(2,2)}/k^1_{p(2,1)}$, respectively, could be determined.

In the above analysis, the best fit was determined by minimizing the sum of squared errors (SSEs) between the experimental data and model predictions. The fitting was performed within MATLAB (R2020a) in two steps: (i) a coarse-grained search and (ii) a trust region reflective optimization. The coarse-grained fitting gave initial order-of-magnitude estimates for the parameters, which were used for identifying upper and lower parameter bounds for the trust region reflective optimization. MATLAB's built-in *lsqnonlin* solver was used to implement the trust region reflective algorithm. The Jacobian matrix generated by the *lsqnonlin* solver was used to estimate the standard error of each parameter, as explained in Sherck et al.[37] As summarized in Table 3, 14 different reaction rate constants were determined in three steps (4 or 5 rate constants were determined at each fitting step); nine of them have been unknown prior to this work. Coarse-grained and trust region reflective optimization methods were used as described in a previous publication.[37]

The experimental data for cumulative number-average lactate and glycolate sequence lengths ($(n_1)_n^{cumu}$ and $(n_2)_n^{cumu}$, respectively) for PLGA copolymers used in our analysis were calculated from ^{13}C NMR data i.e., from the cumulative relative molar concentrations of lactate−**lactate**−lactate, lactate−**lactate**−glycolate (or glycolate−**lactate**−lactate), lactate−**glycolate**−glycolate (or glycolate−**glycolate**−lactate), and glycolate−**glycolate**−glycolate triads (I_{111}^{cumu}, I_{112}^{cumu} (=I_{211}^{cumu}), I_{122}^{cumu} (=I_{221}^{cumu}), and I_{222}^{cumu}, respectively) determined by ^{13}C NMR reported in Qian et al.[42] using the following equations

$$(n_1)_n^{cumu} \cong 2\frac{I_{111}^{cumu}}{I_{112}^{cumu}} + 2 \tag{1}$$

$$(n_2)_n^{cumu} \cong 2\frac{I_{222}^{cumu}}{I_{122}^{cumu}} + 2 \tag{2}$$

The derivations of these equations are presented in Section S6 of the SI. Note that these equations are the same as those used in Qian et al.[42]

These experimental $(n_1)_n^{cumu}$ and $(n_2)_n^{cumu}$ data were compared with predictions of the kinetic model. In model calculations, the lactate and glycolate sequence lengths ($(n_1)_n^{cumu}$ and $(n_2)_n^{cumu}$, respectively) were calculated using the following equations[43]

$$(N_i)_n^{inst}\left(=\frac{(n_i)_n^{inst}}{2}\right) = \frac{1}{1-P_{ii}} \tag{3}$$

$$(N_i)_w^{inst}\left(=\frac{(n_i)_w^{inst}}{2}\right) = \frac{1+P_{ii}}{1-P_{ii}} \tag{4}$$

https://doi.org/10.1021/acs.iecr.1c03096
Ind. Eng. Chem. Res. 2021, 60, 14685−14700

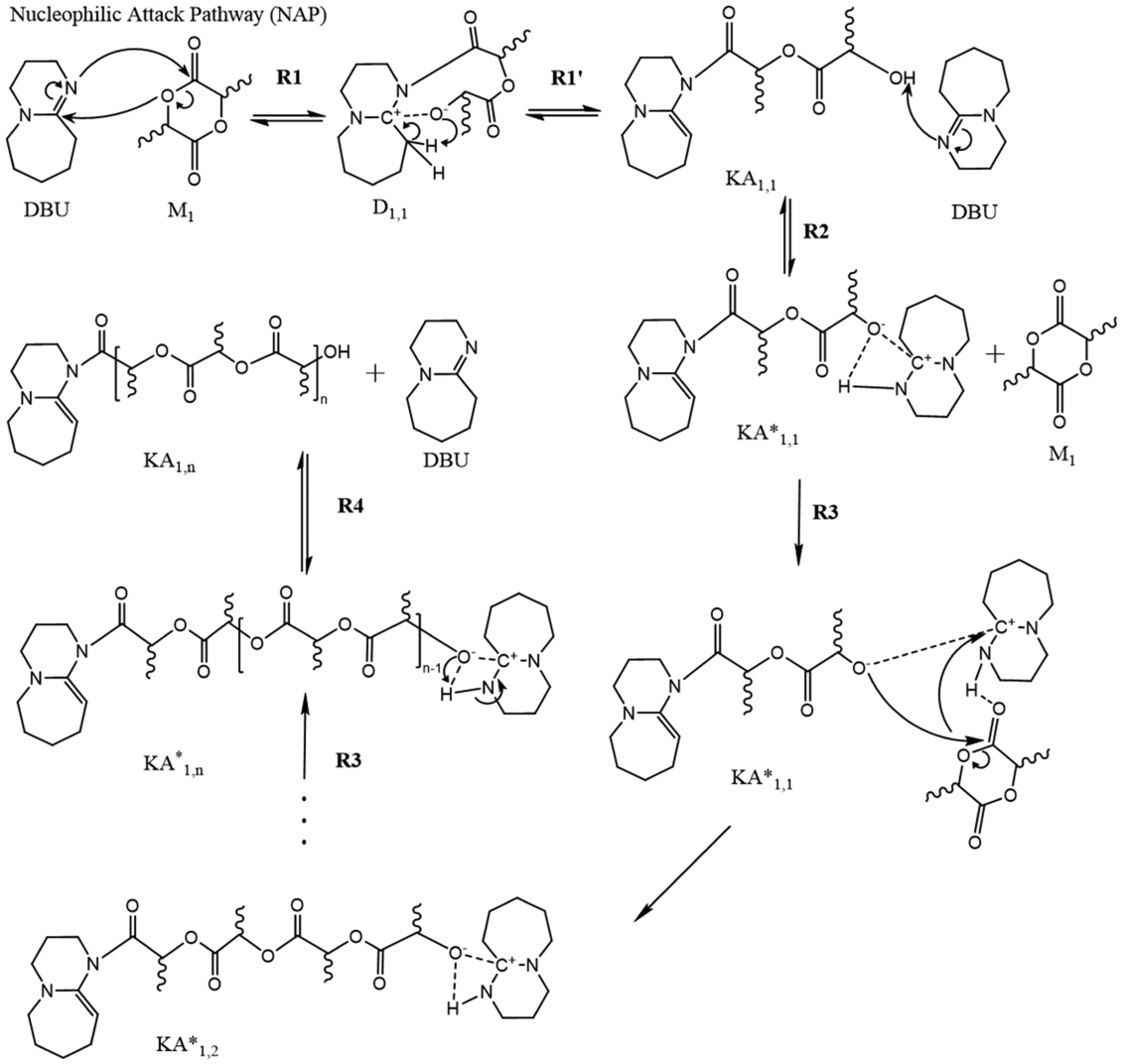

Figure 3. Reactions (R1−R4) and species involved in the nucleophilic attack pathway (NAP) of the DBU-catalyzed ROP of lactide (LA) (M_1). These reaction steps were derived from data reported in various papers, as discussed in detail in our previous publication;[37] this figure is an upgraded version of the NAP reaction network diagram reported in Sherck et al.[37] (see the text for details). An identical set of reactions are assumed for the DBU-catalyzed copolymerization of LA and glycolide (GL) (M_2). Reaction notations (e.g., "R1") are the same as in Figure 6.

$$(N_i)_n^{\text{cumu}}\left(= \frac{(n_i)_n^{\text{cumu}}}{2}\right) = \frac{\int_0^p F_i \, dp}{\int_0^p \frac{F_i}{(N_i)_n^{\text{inst}}} dp} \tag{5}$$

$$(N_i)_w^{\text{cumu}}\left(= \frac{(n_i)_w^{\text{cumu}}}{2}\right) = \frac{\int_0^p (N_i)_w^{\text{inst}} F_i \, dp}{\int_0^p F_i \, dp} \tag{6}$$

where N_i denotes the monomer sequence length (i = 1 (LA) or 2 (GL)), n_i denotes the repeat unit sequence length (i = 1 (lactate) or 2 (glycolate)), the superscripts, "inst" and "cumu", stand for instantaneous and cumulative, respectively, the subscripts, "n" and "w", stand for number-average and weight-average, respectively, P_{ij} denotes the probability of adding monomer j to a chain end containing monomer i (i, j = 1 (LA) or 2 (GL)), p denotes the overall monomer conversion due to propagation reactions, and F_i denotes the instantaneous copolymer composition. The homopropagation probability P_{ii} is given as follows

$$P_{ii} = \frac{k^1_{p(i,i)}[M_i]}{k^1_{p(i,i)}[M_i] + k^1_{p(i,j)}[M_j]} \tag{7}$$

where $[M_i]$ is the concentration of monomer i. The monomer conversion due to propagation p is given as follows

$$p = \frac{\Delta([N_1])_{\text{prop}} + \Delta([N_2])_{\text{prop}}}{[N_1]_0 + [N_2]_0} \tag{8}$$

where $\Delta([N_i])_{\text{prop}}$ is the cumulative number of moles of monomer i molecules consumed by propagation reactions, and $[N_i]_0$ is the total number of moles of monomer i molecules added to the reactor. The instantaneous copolymer composition F_i is given as

$$F_i = \frac{d[M_i]_{\text{prop}}}{d[M_i]_{\text{prop}} + d[M_j]_{\text{prop}}} \tag{9}$$

where $d[M_i]_{\text{prop}}$ is the differential change in concentration of monomer i due to propagation reactions; of note, the $d[M_i]$ notation (without the subscript "prop") used in eqs 10−12, 15,

https://doi.org/10.1021/acs.iecr.1c03096
Ind. Eng. Chem. Res. 2021, 60, 14685−14700

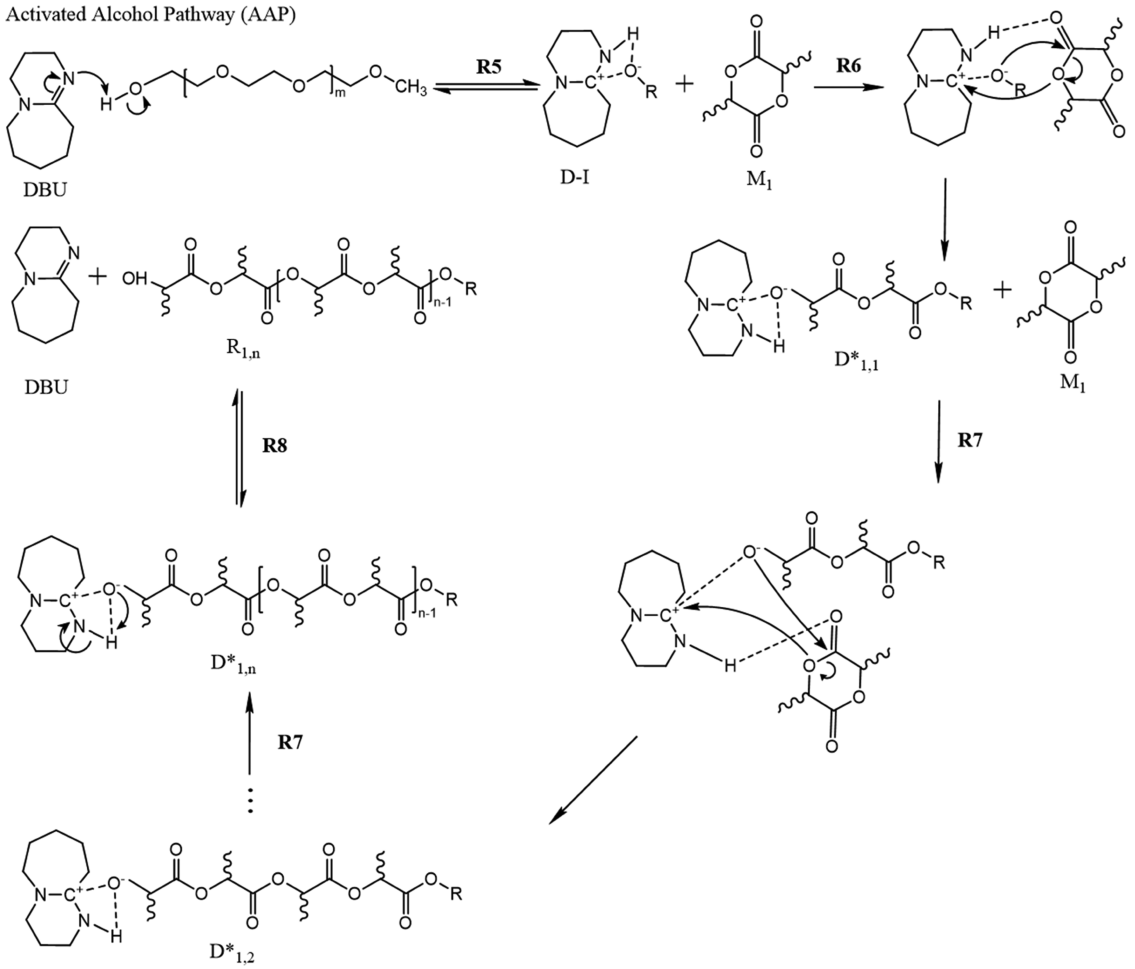

Figure 4. Reactions (R5−R8) and species involved in the activated alcohol pathway (AAP) of the DBU-catalyzed ROP of LA (M_1); these reaction steps were derived from data reported in various papers, as discussed in detail in our previous publication.[37] An identical set of reactions are assumed for the DBU-catalyzed copolymerization of LA and GL (M_2). Reaction notations (e.g., "R5") are the same as in Figure 6.

and 16 denotes the overall differential change in concentration of monomer *i*. Note that the LA (or GL) monomer sequence length ("N_i") is a half of the lactate (or glycolate) sequence length ("n_i") because when polymerized, each LA (or GL) monomer turns into two lactate (or glycolate) repeat units.

3. EXPERIMENTAL SECTION

3.1. Materials. *Rac*-lactide (LA), mPEG-OH (monohydroxy monomethyl ether poly(ethylene glycol), M_n = 2000 g/mol), benzoic acid, and 1,8-diazabicyclo[5.4.0]undec-7-ene (DBU) were purchased from Sigma-Aldrich. Glycolide (GL) was purchased from TCI America. $CDCl_3$ was purchased from Cambridge Isotope Laboratories. PLGA copolymerization reactions were performed at ambient temperature (=22 ± 1 °C).

3.2. Batch Copolymerization of LA and GL. Reactions were conducted under a N_2 atmosphere. The monomers (70 mg of LA and 14 mg of GL) and initiator (80 mg of mPEG-OH) were dissolved in 7.0 mL of $CDCl_3$. The polymerization was initiated by the injection of 1.0 μL of DBU (catalyst) dissolved in 1 mL of $CDCl_3$ at t = 0. At designated times, 1 mL of the reaction mixture was taken from the reactor and transferred to a vial containing 10 mg of benzoic acid to terminate the polymerization reaction. For the different time points, the amounts of unreacted LA (two protons per monomer at 5.12−4.97 ppm) and GL (four protons per monomer at 4.97−4.90 ppm) relative to the amount of polymerized LA (two protons per monomeric unit at 5.28−5.12 ppm) and polymerized GA (four protons per monomeric unit at 4.90−4.65 ppm) were determined by ^{1}H NMR using a Bruker AV-III-400-HD spectrometer with $CDCl_3$ as a solvent; representative NMR spectra are presented in Figure S1 of the Supporting Information (SI).

4. RESULTS AND DISCUSSION

4.1. Copolymerization Reaction Mechanisms and Kinetic Modeling. In the present study, the reaction scheme for the DBU-catalyzed copolymerization of LA and GL was derived from that for the DBU-catalyzed homopolymerization of LA,[37] assuming that due to their chemical similarity, GL undergoes a similar set of reactions to those observed with LA. As summarized in Figures 3−6, the copolymerization process involves four different types of reactions: (i) initiation via the nucleophilic attack pathway (NAP) and subsequent propagation (Figure 3), (ii) initiation via the activated alcohol pathway (AAP) and subsequent propagation (Figure 4), (iii) inter- and intrachain combinations via the acylation of ketene aminals (Figure 5A), and (iv) cascadic deactivation of DBU due to acids (Figure 5B). The initiation of the NAP involves DBU's nucleophilic attack of the ester carbonyl on the LA (or

https://doi.org/10.1021/acs.iecr.1c03096
Ind. Eng. Chem. Res. 2021, 60, 14685−14700

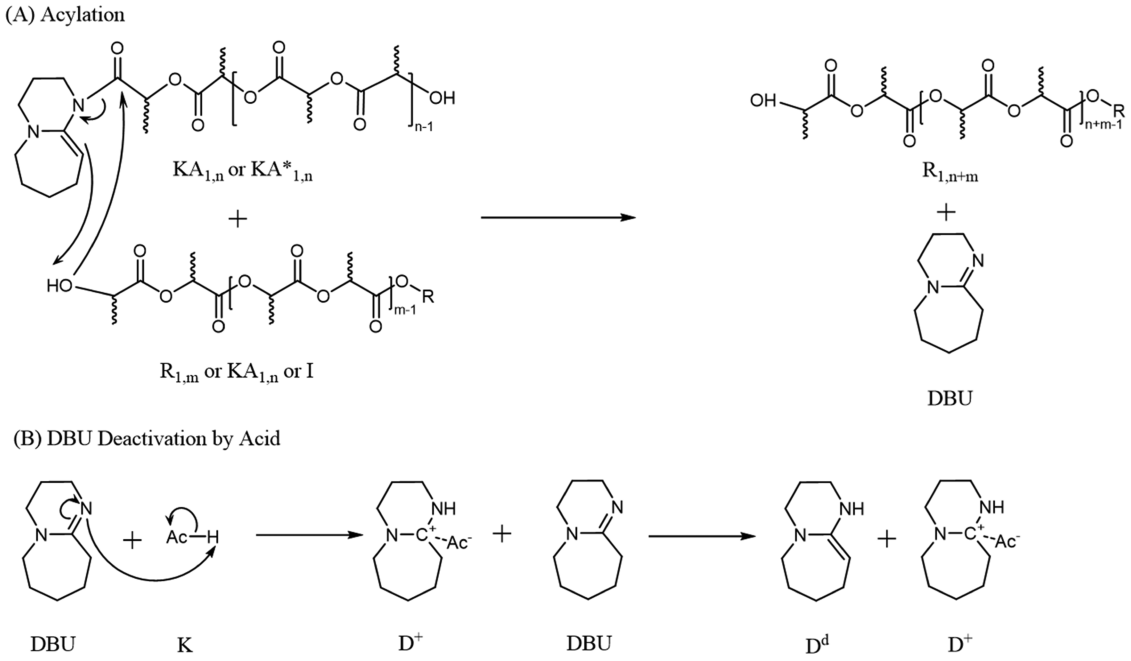

Figure 5. Reactions and species involved in the (A) acylation and (B) DBU deactivation processes of the DBU-catalyzed ROP of LA; these reaction steps were derived from data reported in various papers, as discussed in detail in our previous publication.[37] Acylation is demonstrated between $KA_{1,n}$ and $R_{1,m}$, but it can occur between any species with a ketene aminal end group and any species with a −OH end group (R9−R16 in Figure 6). Identical reactions are assumed for the DBU-catalyzed copolymerization of LA and GL. DBU deactivation occurs through a cascade of steps (R26).

GL) ring (Figure 3), whereas the activation of the AAP is due to the hydrogen-bond complexation between DBU and the hydroxyl end group of the initiator (or a chain) (Figure 4). For the DBU-catalyzed homopolymerization of LA, the relative strength of the two pathways was found to be controlled by the initiator (alcohol)-to-catalyst (DBU) ratio;[37] in excess alcohol initiator, the polymerization occurred predominantly through the AAP and, as a result, exhibited a "living" characteristic, whereas in excess DBU relative to the initiator, the polymerization occurred through the NAP and exhibited a "chain growth" characteristic because of the existence of combination reactions (Figure 5). The complexity associated with analyzing the kinetics of the LA and GL copolymerization lies in the fact that the numbers of kinetic equations and rate constants we have to deal with become quadrupled relative to the LA (or GL) homopolymerization case; strategies used for dealing with this difficulty will be discussed in Section 4.2. Before that, below we discuss further details of the reactions that are considered in our analysis of the kinetics of the DBU-catalyzed LA and GL copolymerization processes.

4.1.1. Modeling of Reactions in the Nucleophilic Attack Pathway (NAP). DBU is a strong nucleophile and thus has a strong tendency to react with the C═O group of LA or GL. The actual electron transfer mechanisms of this and other associated reactions in this NAP are summarized in Figure 3. Note that Figure 3 is an updated version of the NAP reaction network diagram reported in our previous publication;[37] an additional reaction step (R1′) and an additional intermediate species ($KA_{1,1}$) have been added, and Reaction #R2 has been revised to be a reversible reaction based on the following reasons. Brown et al.[34] have speculated the conversion process from $D_{1,1}$ to $KA_{1,1}$ (Reaction #R1′) to be an irreversible reaction based on the large enthalpy change associated with this reaction, which previously led us to treat this reaction as an irreversible one.[37] However, if the R1′ reaction is irreversible, the entire process of generating $KA_{1,1}$ becomes an irreversible process, which contradicts with data reported in Carafa et al.[39] and Kers et al.;[47] therefore, R1′ must be treated as a reversible reaction. Carafa et al.[39] stated that NMR could not detect any intermediate species for $KA_{1,1}$; therefore, $D_{1,1}$ must be, at most, a short-lived intermediate. Also, in our previous study,[37] we found no evidence of zwitterionic polymerization initiation due to $D_{1,1}$ (speculated by Brown et al.[34]). For these reasons, $D_{1,1}$ was not included in our kinetic model. $D_{1,1}$ is shown above for completeness. As shown in Figure 6, NAP-related kinetic parameters include the rate constants for association and dissociation between DBU and LA (or GL) (k^2_{a1}, k^2_{d1}, k^2_{a2}, and k^2_{d2}; to be determined by fitting with LA/GL homopolymerization data (Figure 7)), the rate constants for association and dissociation between DBU and an interacting −OH species containing an LA (or GL) monomer adjacent to the OH end group (k^1_{a1}, k^1_{d1}, k^1_{a2}, and k^1_{d2}; to be determined by fitting with LA/GL homopolymerization data (Figure 7)), the homopropagation rate constants ($k^1_{p(1,1)}$ and $k^1_{p(2,2)}$; to be determined by fitting with LA/GL homopolymerization data (Figure 7)), and the cross-propagation rate constants ($k^1_{p(1,2)}$ and $k^1_{p(2,1)}$; to be determined by fitting with LA + GL copolymerization data (Figure 8)). Typically, rate constants were determined in two steps; first, a coarse-grained fitting was performed to identify parameter bounds, and then a trust region reflective optimization was performed to find least-squares fit parameters. Initial guesses were based on the parameters reported in Sherck et al.[37]

4.1.2. Modeling of Reactions in the Activated Alcohol Pathway (AAP). Figure 4 displays all reactions involved in the AAP. This pathway begins with the complexation of DBU with the alcohol initiator via hydrogen bonding. The DBU−alcohol complex ($[D{-}I]$) reacts with LA or GL to form a propagating

https://doi.org/10.1021/acs.iecr.1c03096
Ind. Eng. Chem. Res. 2021, 60, 14685−14700

Initiation/Propagation:

Nucleophilic Attack Pathway (NAP)

$$(R1.1)\ D + M_1 \underset{k^2_{a1}}{\overset{k^2_{a1}}{\rightleftharpoons}} \left(D_{1,1} \rightleftharpoons\right) KA_{1,1}$$

$$(R\,1.2)\ D + M_2 \underset{k^2_{a2}}{\overset{k^2_{a2}}{\rightleftharpoons}} \left(D_{2,1} \rightleftharpoons\right) KA_{2,1}$$

$$(R\,2.1)\ KA_{1,1} + D \underset{k^1_{d1}}{\overset{k^1_{a1}}{\rightleftharpoons}} KA^*_{1,1}$$

$$(R\,2.2)\ KA_{2,1} + D \underset{k^1_{d2}}{\overset{k^1_{a2}}{\rightleftharpoons}} KA^*_{2,1}$$

$$(R\,3.1)\ KA^*_{1,m-1} + M_1 \xrightarrow{k^1_{p(1,1)}} KA^*_{1,m}$$

$$(R\,3.2)\ KA^*_{2,m-1} + M_1 \xrightarrow{k^1_{p(2,1)}} KA^*_{1,m}$$

$$(R\,3.3)\ KA^*_{1,m-1} + M_2 \xrightarrow{k^1_{p(1,2)}} KA^*_{2,m}$$

$$(R\,3.4)\ KA^*_{2,m-1} + M_2 \xrightarrow{k^1_{p(2,1)}} KA^*_{2,m}$$

$$(R\,4.1)\ KA^*_{1,m} \underset{k^1_{d1}}{\overset{k^1_{a1}}{\rightleftharpoons}} KA_{1,m} + D$$

$$(R\,4.2)\ KA^*_{2,m} \underset{k^1_{d2}}{\overset{k^1_{a2}}{\rightleftharpoons}} KA_{2,m} + D$$

Activated Alcohol Pathway (AAP)

$$(R\,5)\ D + I \underset{k^2_d}{\overset{k^2_a}{\rightleftharpoons}} [D-I]$$

$$(R\,6.1)\ [D-I] + M_1 \xrightarrow{k_{i1}} D^*_{1,1}$$

$$(R\,6.2)\ [D-I] + M_2 \xrightarrow{k_{i2}} D^*_{2,1}$$

$$(R\,7.1)\ D^*_{1,n-1} + M_1 \xrightarrow{k^1_{p(1,1)}} D^*_{1,n}$$

$$(R\,7.2)\ D^*_{2,n-1} + M_1 \xrightarrow{k^1_{p(2,1)}} D^*_{1,n}$$

$$(R\,7.3)\ D^*_{1,n-1} + M_2 \xrightarrow{k^1_{p(1,2)}} D^*_{2,n}$$

$$(R\,7.4)\ D^*_{2,n-1} + M_2 \xrightarrow{k^1_{p(2,2)}} D^*_{2,n}$$

$$(R\,8.1)\ D^*_{1,n} \underset{k^1_{d1}}{\overset{k^1_{a1}}{\rightleftharpoons}} R_{1,n} + D$$

$$(R\,8.2)\ D^*_{2,n} \underset{k^1_{d2}}{\overset{k^1_{a2}}{\rightleftharpoons}} R_{2,n} + D$$

Acylation:

Combination

$$(R\,9.1)\ KA^*_{1,n} + I \xrightarrow{k^1_{ac1}} D^*_{1,n} + D$$

$$(R\,9.2)\ KA^*_{2,n} + I \xrightarrow{k^1_{ac2}} D^*_{2,n} + D$$

$$(R\,10.1)\ KA^*_{1,n} + R_{1,m} \xrightarrow{k^1_{ac1}} D^*_{1,m+n} + D$$

$$(R\,10.2)\ KA^*_{2,n} + R_{1,m} \xrightarrow{k^1_{ac2}} D^*_{2,m+n} + D$$

$$(R\,10.3)\ KA^*_{1,n} + R_{2,m} \xrightarrow{k^1_{ac1}} D^*_{1,m+n} + D$$

$$(R\,10.4)\ KA^*_{2,n} + R_{2,m} \xrightarrow{k^1_{ac2}} D^*_{2,m+n} + D$$

$$(R\,11.1)\ KA^*_{1,n} + KA_{1,m} \xrightarrow{k^1_{ac1}} KA^*_{1,m+n} + D$$

$$(R\,11.2)\ KA^*_{2,n} + KA_{1,m} \xrightarrow{k^1_{ac2}} KA^*_{2,m+n} + D$$

$$(R\,11.3)\ KA^*_{1,n} + KA_{2,m} \xrightarrow{k^1_{ac1}} KA^*_{1,m+n} + D$$

$$(R\,11.4)\ KA^*_{2,n} + KA_{2,m} \xrightarrow{k^1_{ac2}} KA^*_{2,m+n} + D$$

$$(R\,12.1)\ KA_{1,n} + KA_{1,m} \xrightarrow{k^1_{ac1}} KA_{1,m+n} + D$$

$$(R\,12.2)\ KA_{2,n} + KA_{1,m} \xrightarrow{k^1_{ac2}} KA_{1,m+n} + D$$

$$(R\,12.3)\ KA_{1,n} + KA_{2,m} \xrightarrow{k^1_{ac1}} KA_{2,m+n} + D$$

$$(R\,12.4)\ KA_{2,n} + KA_{2,m} \xrightarrow{k^1_{ac2}} KA_{2,m+n} + D$$

$$(R\,13.1)\ KA_{1,n} + I \xrightarrow{k^1_{ac1}} R_{1,n} + D$$

$$(R\,13.2)\ KA_{2,n} + I \xrightarrow{k^1_{ac2}} R_{2,n} + D$$

Acylation:

Combination (Continued)

$$(R\,14.1)\ KA_{1,n} + R_{1,m} \xrightarrow{k^1_{ac1}} R_{1,n+m} + D$$

$$(R\,14.2)\ KA_{2,n} + R_{1,m} \xrightarrow{k^1_{ac2}} R_{2,n+m} + D$$

$$(R\,14.3)\ KA_{1,n} + R_{2,m} \xrightarrow{k^1_{ac1}} R_{1,n+m} + D$$

$$(R\,14.4)\ KA_{2,n} + R_{2,m} \xrightarrow{k^1_{ac2}} R_{2,n+m} + D$$

Cyclization

$$(R\,15.1)\ KA_{1,n} \xrightarrow{k^2_{ac1}} C_{1,n} + D\ (n > 1)$$

$$(R\,15.2)\ KA_{2,n} \xrightarrow{k^2_{ac2}} C_{2,n} + D\ (n > 1)$$

$$(R\,16.1)\ KA_{1,1} \xrightarrow{k^2_{ac1}} M_1 + D$$

$$(R\,16.2)\ KA_{2,1} \xrightarrow{k^2_{ac2}} M_2 + D$$

DBU Deactivation:

$$(R\,17.1)\ D^*_{1,n} + K \xrightarrow{k^1_t} R_{1,n} + D^d$$

$$(R\,17.2)\ D^*_{2,n} + K \xrightarrow{k^1_t} R_{2,n} + D^d$$

$$(R\,18.1)\ KA^*_{1,m} + K \xrightarrow{k^1_t} KA_{1,m} + D^d$$

$$(R\,18.2)\ KA^*_{2,m} + K \xrightarrow{k^1_t} KA_{2,m} + D^d$$

$$(R\,19.1)\ D^*_{1,n} + D^*_{1,m} \xrightarrow{k_d} R_{1,m} + D^*_{1,n} + D^d$$

$$(R\,19.2)\ D^*_{2,n} + D^*_{1,m} \xrightarrow{k_d} R_{1,m} + D^*_{2,n} + D^d$$

$$(R\,19.3)\ D^*_{1,n} + D^*_{2,m} \xrightarrow{k_d} R_{2,m} + D^*_{1,n} + D^d$$

$$(R\,19.4)\ D^*_{2,n} + D^*_{2,m} \xrightarrow{k_d} R_{2,m} + D^*_{2,n} + D^d$$

$$(R\,20.1)\ D^*_{1,n} + KA^*_{1,m} \xrightarrow{k_d} KA_{1,m} + D^*_{1,n} + D^d$$

$$(R\,20.2)\ D^*_{2,n} + KA^*_{1,m} \xrightarrow{k_d} KA_{1,m} + D^*_{2,n} + D^d$$

$$(R\,20.3)\ D^*_{1,n} + KA^*_{2,m} \xrightarrow{k_d} KA_{2,m} + D^*_{1,n} + D^d$$

$$(R\,20.4)\ D^*_{2,n} + KA^*_{2,m} \xrightarrow{k_d} KA_{2,m} + D^*_{2,n} + D^d$$

$$(R\,21.1)\ KA^*_{1,n} + D^*_{1,m} \xrightarrow{k_d} R_{1,m} + KA^*_{1,n} + D^d$$

$$(R\,21.2)\ KA^*_{2,n} + D^*_{1,m} \xrightarrow{k_d} R_{1,m} + KA^*_{2,n} + D^d$$

$$(R\,21.3)\ KA^*_{1,n} + D^*_{2,m} \xrightarrow{k_d} R_{2,m} + KA^*_{1,n} + D^d$$

$$(R\,21.4)\ KA^*_{2,n} + D^*_{2,m} \xrightarrow{k_d} R_{2,m} + KA^*_{2,n} + D^d$$

$$(R\,22.1)\ KA^*_{1,n} + KA^*_{1,m} \xrightarrow{k_d} KA_{1,m} + KA^*_{1,n} + D^d$$

$$(R\,22.2)\ KA^*_{2,n} + KA^*_{1,m} \xrightarrow{k_d} KA_{1,m} + KA^*_{2,n} + D^d$$

$$(R\,22.3)\ KA^*_{1,n} + KA^*_{2,m} \xrightarrow{k_d} KA_{2,m} + KA^*_{1,n} + D^d$$

$$(R\,22.4)\ KA^*_{2,n} + KA^*_{2,m} \xrightarrow{k_d} KA_{2,m} + KA^*_{2,n} + D^d$$

$$(R\,23.1)\ D^*_{1,n} \xrightarrow{k^2_t} R_{1,n} + D^d$$

$$(R\,23.2)\ D^*_{2,n} \xrightarrow{k^2_t} R_{2,n} + D^d$$

$$(R\,24.1)\ KA^*_{1,m} \xrightarrow{k^2_t} KA_{1,m} + D^d$$

$$(R\,24.2)\ KA^*_{2,m} \xrightarrow{k^2_t} KA_{2,m} + D^d$$

$$(R\,25)\ D + K \xrightarrow{k^3_t} D^d$$

Cascade

$$(R\,26)\ D + K \xrightarrow{k^4_t} D^+ + D \xrightarrow{k^5_t} D^+ + D^d$$

Figure 6. Reaction mechanisms associated with the DBU-catalyzed ROP of LA and GL, including the reaction pathways described in Figure 3 (NAP), 4 (AAP), and 5 (acylation and DBU deactivation). Differential equations describing the kinetics of these reactions are summarized in Sections S1−S5 of the Supporting Information (SI).

chain ($D^*_{1,1}$), which contains a "DBU$^+$" group at one end and an initiator fragment ("−OR") at the other end. This AAP pathway ends when the DBU$^+$ end group of a propagating chain becomes dissociated into DBU and a hydroxyl group.

https://doi.org/10.1021/acs.iecr.1c03096
Ind. Eng. Chem. Res. 2021, 60, 14685−14700

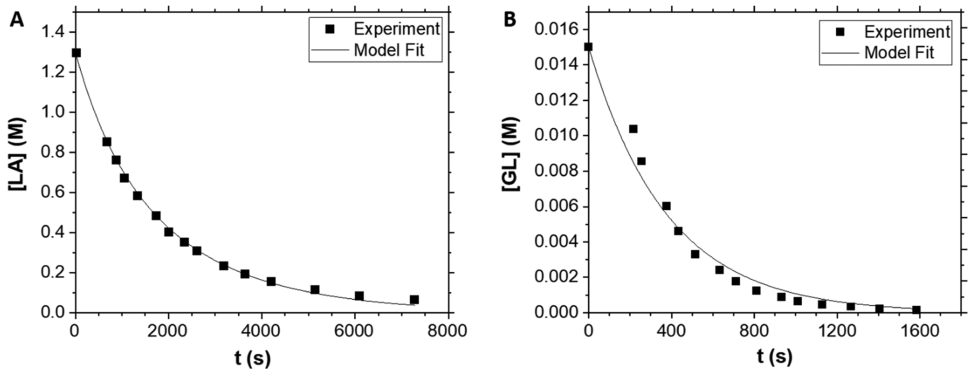

Figure 7. Monomer conversion data for the DBU-catalyzed batch homopolymerization of (A) LA and (B) GL taken from Qian et al.[42] The polymerization reaction conditions used were as follows: (A) $[LA]_o$ = 1.32 M, $[ROH]_o$ = 5.00 mM, $[DBU]_o$ = 6.60 mM, solvent = $CDCl_3$, and T = 25 °C; and (B) $[GL]_o$ = 15.0 mM, $[ROH]_o$ = 5.10 mM, $[DBU]_o$ = 33.7 μM, solvent = $CDCl_3$, and T = 25 °C. The data in panel (A) were fit to our kinetic model described in Sections S1−S5 of the SI (only the LA homopolymerization equations) using $k^1_{p(1,1)}$, k^2_{a1}, k^2_{d1}, k^1_{a1}, and k^1_{d1} as fitting parameters; the best-fit values are summarized in Table 1A. The data in panel (B) were fit to our kinetic model described in Sections S1−S5 of the SI (only the GL homopolymerization equations) using $k^1_{p(2,2)}$, k^2_{a2}, k^2_{d2}, k^1_{a2}, and k^1_{d2} as fitting parameters; the best-fit values are summarized in Table 1B.

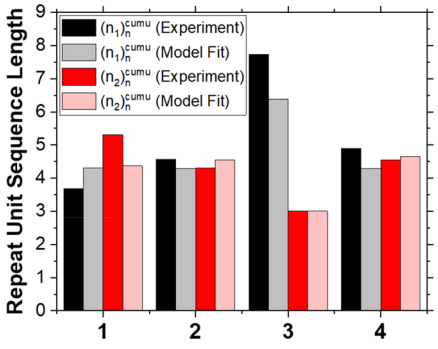

Figure 8. Cumulative number-average repeat unit (lactate (L) or glycolate (G)) sequence length data for the DBU-catalyzed semibatch copolymerization of LA and GL taken from Qian et al.[42] The target molecular weights and copolymerization reaction conditions used were as follows: (1) target = PEG_{5k} − $PL_{2.5k}G_{2.5k}A$, $[LA]_o$ = 144 mM (reactor), $[ROH]_o$ = 4.28 mM (reactor), $[DBU]_o$ = 73.7 mM (reactor), solvent = dichloromethane (DCM) (reactor), $[GL]_o$ = 144 mM (feed stream), solvent = THF (feed stream), $\dot{v}$ = 3.34 × 10^{-3} mL/s (feed stream), and T = 25 °C (reactor/feed stream); (2) target = PEG_{5k} − $PL_{5k}G_{5k}A$, $[LA]_o$ = 300 mM (reactor), $[ROH]_o$ = 4.28 mM (reactor), $[DBU]_o$ = 73.7 mM (reactor), solvent = DCM (reactor), $[GL]_o$ = 300 mM (feed stream), solvent = THF (feed stream), $\dot{v}$ = 3.34 × 10^{-3} mL/s (feed stream), and T = 25 °C (reactor/feed stream); (3) target = PEG_{5k} − $PL_{7.5k}G_{2.5k}A$, $[LA]_o$ = 450 mM (reactor), $[ROH]_o$ = 4.28 mM (reactor), $[DBU]_o$ = 73.7 mM (reactor), solvent = DCM (reactor), $[GL]_o$ = 150 mM (feed stream), solvent = THF (feed stream), $\dot{v}$ = 3.34 × 10^{-3} mL/s (feed stream), and T = 25 °C (reactor/feed stream); and (4) target = PEG_{5k} − $PL_{7.5k}G_{7.5k}A$, $[LA]_o$ = 433 mM (reactor), $[ROH]_o$ = 4.28 mM (reactor), $[DBU]_o$ = 73.7 mM (reactor), solvent = DCM (reactor), $[GL]_o$ = 433 mM (feed stream), solvent = THF (feed stream), $\dot{v}$ = 3.34 × 10^{-3} mL/s (feed stream), and T = 25°C (reactor/feed stream). These sequence length data were simultaneously fit to our semibatch copolymerization model described in Sections S1−S5 of the SI and Section 4.4 of the main text using $k^1_{p(1,2)}$, $k^1_{p(2,1)}$, k^2_{ac1}, and k^2_{ac2} as fitting parameters; for LA and GL homopolymerization reactions, the rate constant values listed in Table 1 were used. The best-fit values for $k^1_{p(1,2)}$, $k^1_{p(2,1)}$, k^2_{ac1}, and k^2_{ac2} are summarized in Table 2.

As shown in Figure 6, there are totally 12 rate constants associated with the AAP, which include the rate constants for association and dissociation between DBU and the hydroxyl end group of the alcohol initiator or a chain (k^1_a = 5.90 × 10^4 s^{-1} M^{-1} and k^1_d = 4.21 × 10^3 s^{-1}; values taken from Sherck et al.[37]), the initiation rate constants (k_{i1} and k_{i2}; assumed to be identical to the respective homopropagation rate constants, i.e., k_{i1} = $k^1_{p(1,1)}$ and k_{i2} = $k^1_{p(2,2)}$, which is justifiable within the terminal model[37]), the homopropagation rate constants ($k^1_{p(1,1)}$ and $k^1_{p(2,2)}$; to be determined by fitting with LA/GL homopolymerization data (Figure 7)), and the cross-propagation rate constants ($k^1_{p(1,2)}$ and $k^1_{p(2,1)}$; to be determined by fitting with LA + GL copolymerization data (Figure 8)).

4.1.3. Modeling of Acylation Reactions Involving Ketene Aminals. Sherck et al. were the first to report a value for the rate constant of the acylation (i.e., combination) reaction in the DBU-catalyzed polymerization of LA (Figures 5A and 6).[37] The acylation reactions involve the ketene aminal (KA)-containing species ($KA^*_{1,1}$, $KA^*_{2,1}$, $KA^*_{1,n}$, $KA^*_{2,n}$, $KA_{1,n}$, and $KA_{2,n}$) that are produced in the NAP (Figures 3 and 6). As shown in Figure 3, there are two types of KA species, and they differ in their end group structures; $KA^*_{1,1}$, $KA^*_{2,1}$, $KA^*_{1,n}$, and $KA^*_{2,n}$ are propagating chains and contain a KA group at one end and a DBU^+ group at the other end, whereas $KA_{1,n}$, and $KA_{2,n}$ are dormant chains and contain a KA group at one end and a −OH group at the other end. As shown in Figure 5A, the acylation reaction occurs between a KA end group (of $KA^*_{1,n}$, $KA^*_{2,n}$, $KA_{1,n}$, or $KA_{2,n}$) and a −OH end group (of I, $R_{1,m}$, $R_{2,m}$, $KA_{1,n}$, or $KA_{2,n}$). Therefore, as summarized in Figure 6, both interchain and intrachain acylation reactions are possible. Accordingly, four different acylation rate constants need to be taken into account: k^1_{ac1} (for interchain acylation (combination) involving $KA^*_{1,n}$ or $KA_{1,n}$; a value of 0.309 s^{-1} M^{-1} reported in Sherck et al.[37]), k^1_{ac2} (for interchain acylation (combination) involving $KA^*_{2,n}$ or $KA_{2,n}$; assumed to be equal to k^1_{ac1}), k^2_{ac1} (for intrachain acylation (cyclization) within $KA_{1,n}$; to be determined by fitting with LA + GL copolymerization data (Figure 8)), and k^2_{ac2} (for intrachain acylation (cyclization) within $KA_{2,n}$; assumed to be equal to k^2_{ac1}). Note in our previous study (i.e., in the analysis of the DBU-catalyzed homopolymerization of LA),[37] we ignored intrachain acylation (cyclization) reactions of KA species (i.e., $KA_{1,n}$). In the present study, the intrachain acylation rate constant, k^2_{ac1} (=k^2_{ac2}), was also included as a fitting parameter

https://doi.org/10.1021/acs.iecr.1c03096
Ind. Eng. Chem. Res. 2021, 60, 14685−14700

in the analysis of the DBU-catalyzed copolymerization of LA and GL (Figure 8). As discussed in Section 4.2, the results confirmed that indeed, $k^2_{ac1}[\sum_{n=1}^{\infty}[R_{1,n}] + \sum_{n=1}^{\infty}[R_{2,n}]]$ ($\approx k^2_{ac1}[ROH]_o$) (intrachain acylation) $\ll$ k^1_{ac1} (interchain acylation) (Table 3).

4.1.4. Modeling of DBU Deactivation Reactions. As shown in Figure 5B, acidic impurities (K) can deactivate DBU by forming a complex compound (D^+), which can further react with another DBU molecule and produce a nonreactive derivative (D^d) in a cascade process (R26 in Figure 6). As summarized in Figure 6 (R17 through R25), there are also other DBU deactivation mechanisms that are possible, including direct (acid-induced) stoichiometric (R17, R18, and R25) and indirect (non-acid-induced) (R19−R24) reactions. In our previous publication,[37] these other (non-cascade) mechanisms (R17−R25) have been shown to be insignificant relative to the cascade mechanism (R26). Even the cascade DBU deactivation mechanism does not significantly influence the estimation of the rate constants; ignoring the cascadic reactions (R26) causes the propagation rate constant ($k^1_{p(1,1)}$) to be underestimated by only about 10%.[37] For these reasons, all DBU deactivation reactions have been left out of the present modeling for simplicity.

4.2. Parameterization of the Kinetic Model. The kinetic model was parameterized by fitting to experimental data reported by Qian et al.[42] As summarized in Table 3, there were 16 rate constants that were needed to be determined to quantitatively model DBU-catalyzed LA + GL copolymerization processes (see Figure 6 for the rate constant definitions). These rate constants were determined using the following steps.

First, monomer conversion data from a DBU-catalyzed *rac*-LA batch homopolymerization experiment[42] were fit with our kinetic model described in Section 4.1 using $k^1_{p(1,1)}$ (homopropagation), k^2_{a1} (association between DBU and LA), k^2_{d1} (dissociation between DBU and LA), k^1_{a1} (association between DBU and an interacting −OH species containing an LA monomer adjacent to the OH group), and k^1_{d1} (dissociation between DBU and an interacting −OH species containing an LA monomer adjacent to the OH group) as fitting parameters (Figure 7A); for simplicity, the rate constants for interchain (R9−R14 in Figure 6) and intrachain (R15−R16) acylation reactions were set to values determined in our previous study (k^1_{ac1} = 0.309 s^{-1} M^{-1} and k^2_{ac1} = 0 s^{-1}).[37] The resultant best-fit values are listed in the upper table of Table 1. Also presented for comparison in the upper table of Table 1 are the values for the same set of rate constants obtained previously via analysis of our own data.[37] As can be seen from the table, the two sets of results were in reasonable agreement, which supports the reasonableness of both results.

Similarly, conversion data from a DBU-catalyzed GL batch homopolymerization reaction[42] were fit to our kinetic model using $k^1_{p(2,2)}$ (homopropagation), k^2_{a2} (association between DBU and GL), k^2_{d2} (dissociation between DBU and GL), k^1_{a2} (association between DBU and an interacting −OH species containing a GL monomer adjacent to the OH group), and k^1_{d2} (dissociation between DBU and an interacting −OH species containing a GL monomer adjacent to the OH group) as fitting parameters (Figure 7B); the interchain acylation constant (k^1_{ac2}) was again set to a value of 0.309 s^{-1} M^{-1}, and the intrachain acylation rate (k^2_{ac2}) was ignored.[37] Note in the study by Qian et al.,[42] from which the data shown in Figure 7B were drawn, the PGA homopolymerization reaction could be carried out to complete conversion without running into the precipitation issue by using very low concentrations of DBU (catalyst) and mPEG-OH (initiator). The best-fit parameters are listed in the lower table of Table 1; the values of these rate constants were previously unknown. It is interesting to note that in these DBU-catalyzed cases, the homopropagation rate of GL ($k^1_{p(2,2)}$ = 1.19 × 10^3 s^{-1} M^{-1} at 25 °C) is about 3 orders of magnitude faster than that of LA ($k^1_{p(1,1)}$ = 1.65 s^{-1} M^{-1} at 25 °C). Also note that a comparable value of the propagation rate constant has been reported for the tin-catalyzed homopolymerization of LA at about 100 °C above room temperature ($k^1_{p(1,1)}$ = 1.25 s^{-1} M^{-1} at 130 °C);[48] the rate of polymerization in the DBU-catalyzed case would be orders of magnitude higher than that in the tin-catalyzed case if they are measured at comparable temperatures.

Table 1. Summary of the (A) LA (Monomer 1) and (B) GL (Monomer 2) Homopolymerization Reaction Rate Constant Values (±Standard Errors) Obtained by the Analysis Described in Figure 7[a]

rate constant	best-fit values in this work	best-fit values in Sherck et al., Macromolecules, 2016
$k^1_{p(1,1)}$	1.65 ± 0.02 (s^{-1} M^{-1})	3.59 (s^{-1} M^{-1})
k^2_{a1}	5.71 × 10^{-4} ± 0.95 × 10^{-4} (s^{-1} M^{-1})	7.91 × 10^{-4} (s^{-1} M^{-1})
k^2_{d1}	207 ± 1 (s^{-1})	152 (s^{-1})
k^1_{a1}	3.00 × 10^4 ± 0.01 × 10^4 (s^{-1} M^{-1})	5.90 × 10^4 (s^{-1} M^{-1})
k^1_{d1}	6.00 × 10^3 ± 0.06 × 10^3 (s^{-1} M^{-1})	4.21 × 10^3 (s^{-1} M^{-1})

rate constant	best-fit values in this work
$k^1_{p(2,2)}$	1.19 × 10^3 ± 0.00 × 10^3 (s^{-1} M^{-1})
k^2_{a2}	1.00 × 10^{-5} ± 0.18 × 10^{-5} (s^{-1} M^{-1})
k^2_{d2}	258 ± 1 (s^{-1})
k^1_{a2}	3.60 × 10^4 ± 0.06 × 10^4 (s^{-1} M^{-1})
k^1_{d2}	4.89 × 10^3 ± 0.05 × 10^3 (s^{-1} M^{-1})

[a] In the upper table, the results are compared with those reported in Sherck et al.[37] The reaction conditions used in the study of Sherck et al.[37] were $[LA]_o$ = 707 mM, $[ROH]_o$ = 49.0 mM, $[DBU]_o$ = 10.0 mM, solvent = $CDCl_3$, and T = 25 °C.

We also note that Qian et al. analyzed the LA and GL batch homopolymerization data using the (pseudo) first-order kinetic equations

$$\frac{d[M_1]}{dt} = -k_{app1}[M_1] \quad (10)$$

$$\frac{d[M_2]}{dt} = -k_{app2}[M_2] \quad (11)$$

from which they obtained the values of the apparent first-order rate constants, k_{app1} = 5.5 × 10^{-4} s^{-1} and k_{app2} = 3.1 × 10^{-3} s^{-1}. However, as can be seen from the full kinetic balance equations for LA and GL (eqs S.1.2.1 and S.1.2.2 in Section S1 of the SI), there is no simple equation one can use to extract $k^1_{p(1,1)}$ and $k^1_{p(2,2)}$ from k_{app1} and k_{app2}, respectively; a full numerical analysis is required (as demonstrated in the present work).

Finally, the remainder of the copolymerization rate constants ($k^1_{p(1,2)}$ (cross-propagation), $k^1_{p(2,1)}$ (cross-propagation), k^2_{ac1} (intrachain acylation), and k^2_{ac2} (intrachain acylation)) were determined by comparing repeat unit sequence data from DBU-catalyzed LA + GL semibatch copolymerization reactions[42] with predictions of the kinetic model (Figure 8); specifically, as displayed in the figure, cumulative number-

https://doi.org/10.1021/acs.iecr.1c03096
Ind. Eng. Chem. Res. 2021, 60, 14685−14700

average repeat unit sequence lengths for four different PEG−PLGA materials produced under constant GL addition rate conditions were used for this fitting. The values of the other 12 rate constants were set to be equal to those obtained from the analysis of the homopolymerization reactions discussed above. Note that the data shown in Figure 7 (taken from Qian et al.[42]) were obtained using $CDCl_3$ as the polymerization solvent, whereas the data shown in Figure 8 (taken from the same reference) were obtained using DCM as the solvent. This means that the authors of this reference[42] implicitly assumed that the LA/GL polymerization kinetics are comparable between $CDCl_3$ and DCM, which is a reasonable assumption considering that these two solvents have similar chemical structures and comparable solubility parameters ($\delta_{CHCl_3} \cong 18.7$ $(J/cc)^{1/2}$ and $\delta_{DCM} \cong 20.2$ $(J/cc)^{1/2}$ at 25 °C);[49] we use this same assumption in our analysis. For modeling the semibatch copolymerization reactions, the original GL balance equation (eq S.1.2.2 of the SI) was modified to a form that takes into account the continuous addition of GL to the reactor

$$\frac{d[M_2]}{dt} = \mathcal{R}_2(t) + (M_2^{add} - [M_2])\frac{\dot{\nu}}{V(t)} \tag{12}$$

where $\mathcal{R}_2(t)$ is the rate of change in GL concentration due to chemical reactions (equal to the right-hand side of eq S.1.2.2), M_2^{add} is the concentration of GL being added to the reactor, $\dot{\nu}$ is the constant volumetric addition rate, and $V(t)$ is the volume of the polymerization mixture ($V(t) = V(t=0) + \int_0^t \dot{\nu} dt$). The term, $-[M_2]\frac{\dot{\nu}}{V(t)}$, accounts for the dilution effect, i.e., the decrease in $[M_2]$ due to the increase in $V(t)$. The same modifications have been made for all other species in their respective kinetic balance equations (i.e., in all equations in Section S1 of the SI). Therefore, the general form of the balance of mass for an arbitrary species (species S) is given by

$$\frac{d[S]}{dt} = \mathcal{R}_S(t) + (S^{add} - [S])\frac{\dot{\nu}}{V(t)} \tag{13}$$

where $\mathcal{R}_S(t)$ is the rate of change in concentration of the species S due to chemical reactions (equal to the quantity on the right-hand side of the respective equation in Section S1 of the SI), and S_{add} is the concentration of species S being added to the reactor (in our case, $S_{add} = 0$ unless $S = M_2$ (GL)). As shown in Figure 8, the agreement between experiment and calculations was very good. The fitting results are summarized in Table 2; note that k^2_{ac1} and k^2_{ac2} were floated separately in the fitting scheme, but their difference was found to be insignificant. Table 3 lists all of the 16 rate constants, 14 determined in the present work and 2 taken from a previous study.

Table 2. Summary of the Cross-Propagation and Acylation Rate Constant Values (±Standard Errors) Obtained by the Analysis Described in Figure 8[a]

rate constant	best-fit values
$k^1_{p(1,2)}$	48.9 ± 7.6 (s^{-1} M^{-1})
$k^1_{p(2,1)}$	88.2 ± 0.0 (s^{-1} M^{-1})
k^2_{ac1}	0.906 ± 0.010 (s^{-1})
k^2_{ac2}	0.906 ± 0.010 (s^{-1})

[a]From these results and the results summarized in Table 1, the reactivity ratios for LA (monomer 1) and GL (monomer 2) are estimated to be r_1 ($\equiv k^1_{p(1,1)}/k^1_{p(1,2)}$) = 3.37 × 10^{-2} and r_2 ($\equiv k^1_{p(2,2)}/k^1_{p(2,1)}$) = 13.6.

From the estimates of the propagation rate constants, $k^1_{p(1,1)}$, $k^1_{p(2,2)}$, $k^1_{p(1,2)}$, and $k^1_{p(2,1)}$, the reactivity ratios for LA and GL ($r_1 \equiv k^1_{p(1,1)}/k^1_{p(1,2)}$ and $r_2 \equiv k^1_{p(2,2)}/k^1_{p(2,1)}$, respectively) were calculated. The values obtained were $r_1 = 3.37 \times 10^{-2}$ and $r_2 = 13.6$ ($r_2/r_1 = 4.04 \times 10^2$) for DBU-catalyzed reactions at room temperature. These results are very different from the values reported for tin-catalyzed reactions at 200 °C, $r_1 = 0.2$, and $r_2 = 2.8$ ($r_2/r_1 = 14$).[25] Large catalyst-dependent changes in monomer selectivity have previously been observed for copolymerization reactions, for instance, of ethylene (1) and propylene (2); $r_2/r_1 \approx 10^1$ for titanium-based catalysts at 70 °C, while $r_2/r_1 \approx 10^5$ for metallocene-based catalysts at 50 °C.[50] Catalysts play an important role in controlling the monomer sequence distribution of copolymers through their influence on monomer reactivity ratios.[51,52]

We note that, for free-radical copolymerization processes, monomer reactivity ratios (r_1 and r_2) can be estimated without calculation of the values of the individual propagation rate constants ($k^1_{p(1,1)}$, $k^1_{p(2,2)}$, $k^1_{p(1,2)}$, and $k^1_{p(2,1)}$). Computational methods have been developed for directly estimating the reactivity ratios from experimental data (e.g., instantaneous/cumulative copolymer compositions,[53] instantaneous sequence length distributions,[54] etc.) using a copolymerization model (e.g., the instantaneous and cumulative copolymer composition equations (called the Mayo−Lewis and Skeist equations, respectively), the terminal or penultimate model equations for triad sequence fractions, etc.).[43] However, we would like to point out that these previous methods are not, in principle, applicable to our DBU-catalyzed LA + GL copolymerization situation because in our case the monomer conversion due to propagation p (defined in eq 8) cannot be experimentally determined; as can be seen from eqs S.1.2.1 and S.1.2.2 of the SI, the propagation reaction conversion p cannot be calculated from the experimental values of the unreacted comonomer composition in the polymerization mixture because of the existence of side reactions (i.e., association/dissociation between DBU and a monomer, and intrachain acylation (cyclization)) that involve consumption and regeneration of the monomers. In our case, the calculation of the individual propagation rate constants is required to determine the reactivity ratios.

Figure 9 displays the instantaneous copolymer composition (F_1) vs feed comonomer composition (f_1) plots for both DBU and tin-catalyzed copolymerization reactions of LA and GL, constructed based on the Mayo−Lewis equation

$$F_1 = \frac{r_1 f_1^2 + r_1 f_2}{r_1 f_1^2 + 2 r_1 f_2 + r_2 f_2^2} \tag{14}$$

where $F_1 = d[M_1]_{prop}/(d[M_1]_{prop}+d[M_2]_{prop})$ (which is the same as eq 9) and $f_1 = [M_1]/([M_1]+[M_2])$. In both cases, because $r_1 < 1$ and $r_2 > 1$, the F_1 vs f_1 curves lie below the azeotropic line ($F_1 = f_1$), and drift causes f_1 to increase with conversion; however, because of the greater discrepancy between r_1 and r_2, a greater negative deviation of the F_1−f_1 curve from the azeotropic line is anticipated for the DBU situation. In the copolymerization with DBU, for instance, to obtain an instantaneous mole fraction of LA in the copolymer of $F_1 = 0.50$, the mole fraction of LA in the monomer mixture must be maintained at $f_1 = 0.95$, whereas in the tin-catalyzed case, a significantly different condition would be required (f_1 =

https://doi.org/10.1021/acs.iecr.1c03096
Ind. Eng. Chem. Res. 2021, 60, 14685−14700

Table 3. Summary of the Values (± Standard Errors) of All of the Reaction Rate Constants Associated with the DBU-Catalyzed Copolymerization of LA and GL at 25 °C Determined in This Work[a]

propagation		association between DBU and a monomer	dissociation between DBU and a monomer	association between DBU and −OH	dissociation between DBU and −OH	interchain acylation between ketene aminal (KA) and −OH*	intrachain acylation between KA and −OH
$k_{p(1,1)}^{1§}$	$k_{p(1,2)}^{1§}$	$k_{a1}^{2§}$	$k_{d1}^{2¶}$	$k_{a1}^{1§}$	$k_{d1}^{1¶}$	$k_{ac1}^{1§}$	$k_{ac1}^{2¶}$
1.65 ± 0.02	48.9 + 7.6	$5.71 \times 10^{-4} \pm 0.95 \times 10^{-4}$	207 ± 1	$3.00 \times 10^{4} \pm 0.01 \times 10^{4}$	$6.00 \times 10^{3} \pm 0.06 \times 10^{3}$	0.309 ± 0.012	0.906 ± 0.010
$k_{p(2,2)}^{1§}$	$k_{p(2,1)}^{1§}$	$k_{a2}^{2§}$	$k_{d2}^{2¶}$	$k_{a2}^{1§}$	$k_{d2}^{1¶}$	$k_{ac2}^{1§}$	$k_{ac2}^{2¶}$
$1.19 \times 10^{3} \pm 0.00 \times 10^{3}$	88.2 ± 0.0	$1.00 \times 10^{-5} \pm 0.18 \times 10^{-5}$	258 ± 1	$3.60 \times 10^{4} \pm 0.06 \times 10^{4}$	$4.89 \times 10^{3} \pm 0.05 \times 10^{3}$	0.309 ± 0.012	0.906 ± 0.010

[a]*Values are taken from a previous study.[37] § In the units of s^{-1} M^{-1}. ¶ In the units of s^{-1}.

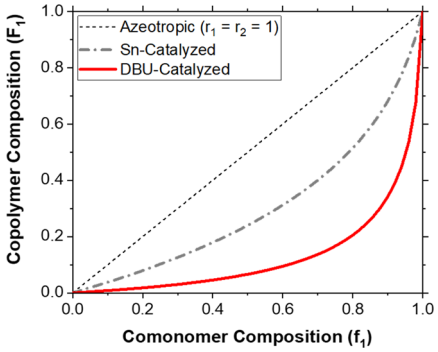

Figure 9. Mayo−Lewis plots for the DBU-catalyzed copolymerization (r_1 = 3.37 × 10^{-2} and r_2 = 13.6 estimated in this work) and Sn-catalyzed copolymerization (r_1 = 0.2 and r_2 = 2.8 reported in Gilding & Reed, Polymer, 1979) of LA (monomer 1) and GL (monomer 2). To obtain an instantaneous mole fraction of LA in the copolymer of F_1 = 0.500, for instance, the mole fraction of LA in the monomer mixture should be maintained at f_1 = 0.953.

0.73). These Mayo−Lewis plots suggest that a PLGA material synthesized using a batch process is expected to have a gradient in composition arranged from mostly GL to almost pure LA along the chain, and such effect will be much greater in DBU-synthesized products than those produced by tin catalysts.

4.3. Limitation of DBU-Catalyzed Batch Copolymerization of LA and GL. The greatest advantage of using DBU is that it enables the room-temperature synthesis of PLGA; at ambient temperatures, transesterification reactions[24] are suppressed, and as a result, polydispersity indices of ≲1.2 are easily achievable. However, the large disparity between r_1 and r_2 in DBU-catalyzed situations is a potential disadvantage; the large difference in reactivity between LA and GL produces a large gradient in monomer composition in a PLGA product synthesized by a batch process ("gradient PLGA"). Long sequences of GL in gradient PLGA chains are problematic because long GL sequences (PGA segments) are insoluble in most organic solvents.[27] This aspect can be discussed quantitatively using the solubility parameter concept as follows. We will consider chloroform ($CHCl_3$) as the solvent. PGA (component "2") is less miscible with $CHCl_3$ (component "3") than PLA (component "1"). Based on their solubility parameter values ($\delta_1 \cong 21.4$ $(J/cc)^{1/2}$, $\delta_2 \cong 23.8$ $(J/cc)^{1/2}$, and $\delta_3 \cong 19.0$ $(J/cc)^{1/2}$, all values at 25 °C),[55,56] the Flory−Huggins interaction parameters are estimated to be $\chi_{13} \cong 0.188$ for PLA/$CHCl_3$ mixtures and $\chi_{23} \cong 0.750$ for PGA/$CHCl_3$ mixtures at 25 °C (based on the molar volume of $CHCl_3$ (≅80.7 cc),[56] $CHCl_3$ is a nonsolvent for PGA). Therefore, if one performs a DBU-catalyzed LA + GL copolymerization using a batch reaction method (i.e., by introducing all monomers into a reactor at the beginning of the process), the growing chains (containing long sequences of GL) will likely precipitate out of the solution at an early stage.

This problem is well demonstrated by the data shown in Figure 10, where experimentally determined monomer conversions were shown to start deviating from predictions of our kinetic model within less than a minute after the initiation of the polymerization. This trend is consistent with the visual observation of a rapid increase in turbidity of the

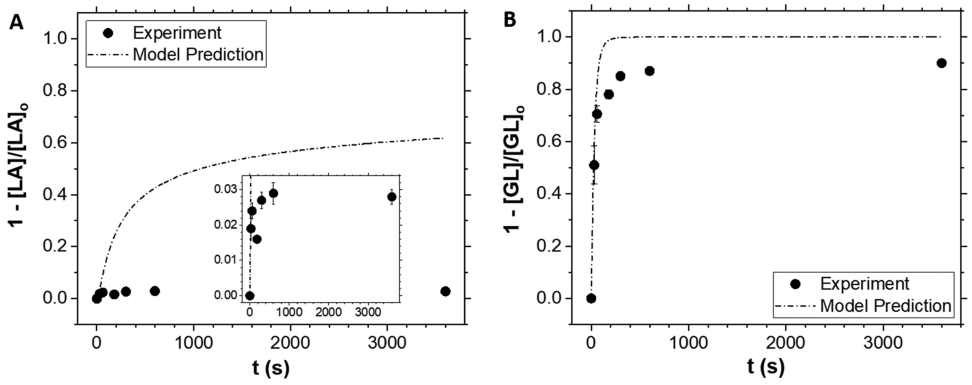

Figure 10. Comparison between experiment and model predictions of (A) LA and (B) GL conversions for the DBU-catalyzed batch copolymerization of LA and GL. The polymerization reaction conditions used were $[LA]_o$ = 60.8 mM, $[GL]_o$ = 15.0 mM, $[ROH]_o$ = 5.00 mM, $[DBU]_o$ = 0.836 mM, solvent = $CDCl_3$, and T = 25 °C. The predictions were calculated based on the kinetic model described in Sections S1−S5 of the SI using the rate constant values listed in Table 3. In panel (A), the inset is a zoom-in view of the plot at lower values of LA conversion. Experiments were performed in triplicate (N = 3). Error bars represent ± standard deviation.

https://doi.org/10.1021/acs.iecr.1c03096
Ind. Eng. Chem. Res. 2021, 60, 14685−14700

polymerization mixture that started at about 3 min into the reaction, which indicates that GL-rich chains indeed became segregated from the solvent ($CHCl_3$) to form large globular masses. Note that the kinetic model itself predicts that the conversion of LA is limited because, in this low-DBU-concentration (AAP-dominant) limit, the chain activation−deactivation equilibrium (R8 in Figure 6) is biased toward the dormant state (i.e., at low $[D]$, $[R_{i,n}] \gg [D^*_{i,n}]$ because $\frac{k_a^1}{k_d^1} = \frac{[D^*_{i,n}]}{[R_{i,n}][D]} = (\text{const})$, where i = 1 (LA) or 2(GL)), and therefore the rate of propagation is limited by the concentration of the alcohol-initiated growing chains ($[D^*_{i,n}]$). Model predictions under different $[ROH]_o$ and $[DBU]_o$ conditions (Figure S2) further support this explanation. Interestingly, Figure 10 suggests that even after the formation of precipitated globules, the polymerization of LA and GL further proceeded (presumably via diffusion of monomers into the polymer droplets) for another 5−10 min before the reaction became completely inhibited due to the mass transfer limitation. A different approach is needed if one wants to synthesize nongradient, statistically monomer sequence-controlled "uniform PLGA" materials while still leveraging the benefits of the DBU chemistry.

Here, we note that "uniform copolymer" is not an IUPAC-accepted term, although it has often been used in the literature; for instance, see Austin and Jacobson[57] and McGrath.[58] Also of note, random copolymer is a different concept. A random copolymer is a copolymer in which the composition of the copolymer is constant throughout the polymerization (because it is produced at an azeotrope and thus contains no composition drift) and equal to the monomer composition in the reactor ($F_1 = f_1$);[59] a random copolymer is an idealized material that can only be produced when the reactivity ratios of the two monomers are both equal to unity ($r_1 = r_2 = 1$).[43] Therefore, random PLGA is not conceptually identical to uniform PLGA because uniform PLGA is produced from the two monomers, LA and GL, which have very disparate reactivities, using a semibatch, time-dependent GL addition method (discussed later in Section 4.4). We define uniform PLGA as nongradient (not deterministically but), statistically sequence-controlled PLGA. According to Lutz,[60] to be qualified as a sequence-controlled polymer, the implementation of the sequence control does not have to be at the deterministic level of resolution.

4.4. Production of Uniform PLGA via Semibatch Copolymerization. Because of the highly distinct reactivities of the two monomers, LA vs GL, under DBU, a uniform PLGA product can only be produced through a semibatch copolymerization process in which the more reactive monomer, GL, needs to be continuously added to compensate for its faster consumption (Figure 11). From a time-dependent version of eq 12

$$\frac{d[M_2]}{dt} = \mathcal{R}_2(t) + (M_2^{add} - [M_2])\frac{\dot{v}(t)}{V(t)} \tag{15}$$

and an equivalent equation for LA

$$\frac{d[M_1]}{dt} = \mathcal{R}_1(t) + (M_1^{add} - [M_1])\frac{\dot{v}(t)}{V(t)} \tag{16}$$

where $\mathcal{R}_1(t)$ is the rate of change in LA concentration due to chemical reactions (equal to the right-hand side of eq S.1.2.1), and M_1^{add} (concentration of LA being added to the reactor) = 0; it can be shown that when the monomer concentration ratio, β ($\equiv [M_2]/[M_1]$), is kept constant, the time-dependent volumetric rate for GL addition is given as

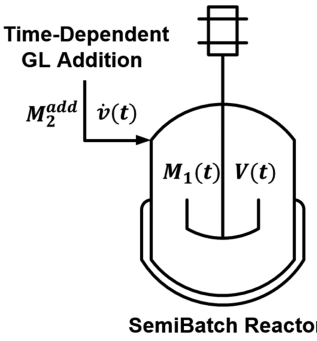

Figure 11. Depiction of a semibatch reactor scheme for engineering PLGA sequences by controlling the time-dependent monomer concentrations in solution; M_2^{add} is the concentration of GL being added to the reactor, $\dot{v}(t)$ is the time-dependent volumetric addition rate, $M_1(t)$ is the concentration of LA inside the reactor, and $V(t)$ is the reactor volume.

$$\dot{v}(t) = -\frac{V(t)}{M_2^{add}}(\mathcal{R}_2(t) - \beta\mathcal{R}_1(t)) \tag{17}$$

These equations (eqs 15−17) have been added to numerical integration routines that can solve for $\dot{v}(t)$ over the course of the polymerization. Note that similar modifications have also been made in the kinetic balance equations for all other species (i.e., in all equations in Section S1 of the SI); to take into account the dilution effect, the following modified kinetic balance equation was used for each species

$$\frac{d[S]}{dt} = \mathcal{R}_S(t) + (S^{add} - [S])\frac{\dot{v}(t)}{V(t)} \tag{18}$$

where the definitions of the notations are the same as for eq 13.

To produce a uniform PLGA, for instance, having a constant average composition of $F_1 = 0.5$ along the chain, the monomer ratio, β, must be maintained at a level of 4.93×10^{-2} throughout the polymerization process (estimated based on the Mayo−Lewis plot in Figure 9). This value was used as an input into eq 17 to estimate the time-dependent rate of GL addition needed for producing the uniform PLGA product. The results of this calculation are presented in Figure 12. As shown in Figure 12A, the resultant $\dot{v}(t)$ profile is highly nonlinear; the volumetric addition rate must be decreased from about 5.80×10^{-2} mL/s to about 2.77×10^{-3} mL/s within the initial 30 s of experiment. In this semibatch (living) copolymerization situation, composition drift is completely eliminated by the continuous addition of GL (Figure 12B). The statistical sequence characteristics are constant along the chain; this polymer product can thus be rightfully called uniform PLGA. For this uniform PLGA, therefore, the cumulative number- and weight-average sequence lengths are identical to their respective instantaneous quantities (Figure 12 E,F). It remains to be explored whether this highly nonlinear, time-dependent monomer addition to the reactor can actually be physically realized at the laboratory scale, for instance, using a programmable syringe pump system. Of note, a conceptually similar but more empirically based approximate approach has previously been proposed in the patent literature.[57] In this patent, a two-step process is proposed; a test copolymerization

https://doi.org/10.1021/acs.iecr.1c03096
Ind. Eng. Chem. Res. 2021, 60, 14685−14700

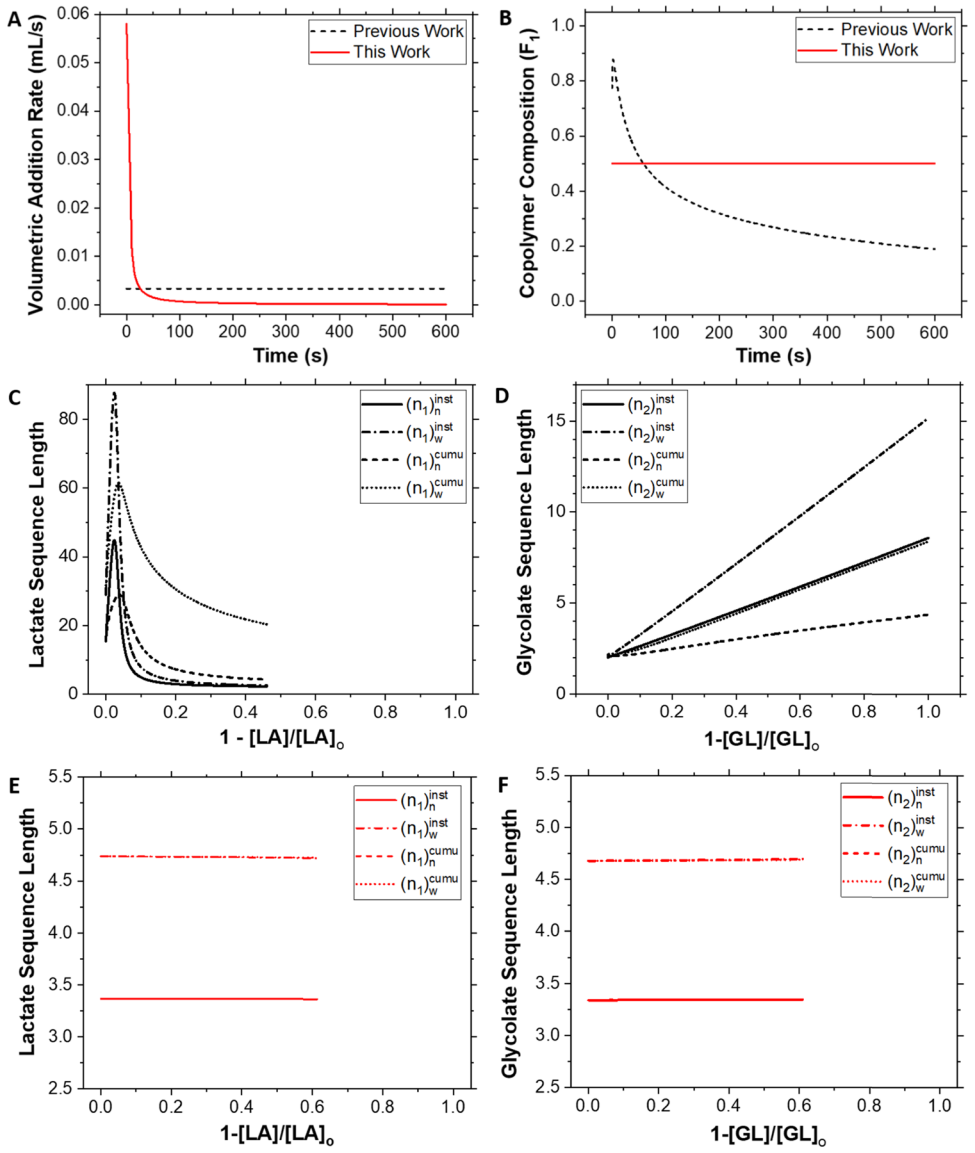

Figure 12. (A) With the kinetically parameterized model (Sections S1−S5 and Table 3), the volumetric addition rate of the GL feed stream ($\dot{v}(t)$) was calculated as a function of time to control the concentration-dependent probabilities of which monomer will add to the growing chain at any instant ("this work"), for the given initial copolymerization reactor and feed stream conditions: target F_1 = 0.5, $[LA]_o$ = 144 mM (reactor), $[GL]_o$ = 7.06 mM (reactor), $[ROH]_o$ = 42.8 mM (reactor), $[DBU]_o$ = 73.7 mM (reactor), solvent = DCM (reactor), $V_{R,o}$ = 2.00 mL (reactor), M_2^{add} = 144 mM (feed stream), solvent = THF (feed stream), and T = 25°C (reactor/feed stream). Qian et al.[42] used a constant volumetric rate for GL addition ($\dot{v} = 3.34 \times 10^{-3}$ mL/s) for the same initial reactor and feed stream conditions ("previous work"). (B) Instantaneous mole fraction of LA in the copolymer (F_1) is calculated as a function of time for PLGA produced by the nonlinear-addition method proposed in panel (A) ("this work"). The result is compared with that for PLGA produced by the constant-addition method used in Qian et al.[42] ("previous work"). Instantaneous/cumulative, number/weight-average, lactic acid/glycolic acid sequence lengths for PLGA produced by (C, D) the constant-addition method ("previous work") versus (E, F) the nonlinear-addition method ("this work"). In panels (E) and (F), the instantaneous quantities are exactly identical to the cumulative quantities (i.e., $(n_i)_n^{inst} = (n_i)_n^{cumu}$ and $(n_i)_w^{inst} = (n_i)_w^{cumu}$ (i = 1, 2)) because there is no drift in the composition of the copolymer throughout the reaction.

reaction is performed with the continuous addition of the more reactive monomer at a constant slow rate, and based on the result of this first reaction, the feed rate of the faster reacting monomer is adjusted in the second step to achieve matched consumption rates between the two monomers. Data reported in this patent document, however, suggest that multiple (more than just one) feedback loops are needed to produce a highly uniform copolymer product.

To avoid the issues associated with batch copolymerization processes (Figure 10), Qian et al. demonstrated a simpler semibatch reactor design, i.e., the addition of GL at a constant volumetric rate (Figure 12A).[42] Figure 12B−D displays the predictions of our model regarding the composition and sequence characteristics of a PLGA thus produced. As shown in these figures, if this constant-addition condition is used, the polymer sequence is no longer controlled. However, the relative simplicity and easiness of this method are certainly appealing.

5. CONCLUSIONS

The present study investigated the kinetics of DBU-catalyzed copolymerization of LA and GL at room temperature. By

https://doi.org/10.1021/acs.iecr.1c03096
Ind. Eng. Chem. Res. 2021, 60, 14685−14700

fitting experimental data to a kinetic model that takes into account all possible reactions (including initiation via activated alcohol and nucleophilic attack pathways, self- and cross-propagation, combination via inter- and intrachain acylation, and DBU deactivation), the hitherto unknown values of 9 different reaction rate constants were determined (Tables 1 and 2). The most remarkable of these results is the 3-orders-of-magnitude difference in the reactivity ratio between LA (r_1 ($\equiv k^1_{p(1,1)}/k^1_{p(1,2)}$) = 3.37 × 10^{-2}) and GL (r_2 ($\equiv k^1_{p(2,2)}/k^1_{p(2,1)}$) = 13.6) (Figure 9). This implies that a PLGA polymer produced by a batch copolymerization process would possess a severe gradient in monomer composition (i.e., from mostly GL to mostly LA) along the chain. In reality, long GL sequences would cause the growing chains to precipitate out of the solution, effectively terminating the chain growth at an early stage of the copolymerization process (Figure 10). Because of the unequal reactivities of the two monomers, LA and GL, a copolymer with a constant average composition along the chain ("uniform PLGA") can only be produced via a semibatch process in which GL needs to be added continuously to compensate for its faster consumption. The analysis based on our kinetic model suggests that if an appropriate time-dependent GL addition condition is used, the PLGA sequence can indeed be controlled; a uniform PLGA can be produced (Figure 12). Using a constant rate of GL addition is unable to eliminate the composition drift during the copolymerization (Figure 12). Further experimental study is warranted to determine the feasibility of the GL addition strategy derived using the kinetic model.

■ ASSOCIATED CONTENT

Supporting Information

The Supporting Information is available free of charge at https://pubs.acs.org/doi/10.1021/acs.iecr.1c03096.

^{1}H NMR spectra for an LA/GL/PLGA mixture (Figure S1); model predictions of LA/GL conversions for DBU-catalyzed batch PLGA copolymerization reactions (Figure S2); kinetic balance equations for the DBU-catalyzed copolymerization of LA and GL in a batch reactor (Section S1); kinetic rate constant definitions (Section S2); mechanisms associated with the kinetic balance equations in Section S1 (Section S3); moment definitions (Section S4); kinetic balance equations in terms of moments (Section S5); and calculation of repeat unit sequence lengths from cumulative relative molar concentrations of repeat unit dyads (Section S6) (PDF)

■ AUTHOR INFORMATION

Corresponding Author

You-Yeon Won − *Davidson School of Chemical Engineering, Purdue University, West Lafayette, Indiana 47907, United States; Purdue University Center for Cancer Research, West Lafayette, Indiana 47906, United States;* orcid.org/0000-0002-8347-6375; Email: yywon@purdue.edu

Authors

Samruddhi Patil − *Davidson School of Chemical Engineering, Purdue University, West Lafayette, Indiana 47907, United States*

Jin Yoo − *Davidson School of Chemical Engineering, Purdue University, West Lafayette, Indiana 47907, United States;* orcid.org/0000-0002-6627-6785

Complete contact information is available at: https://pubs.acs.org/10.1021/acs.iecr.1c03096

Notes

The authors declare no competing financial interest.

■ ACKNOWLEDGMENTS

The authors thank the National Science Foundation (NSF) of the United States for providing financial support for this research (CBET-1803968) and the Ministry of Education of the Korean Government for the National Research Foundation of Korea (NRF) Postdoctoral Fellowship (granted to J.Y., 2020R1A6A3A03037188). The authors also acknowledge support from the Purdue University Center for Cancer Research (PCCR) via an NIH NCI grant (P30 CA023168), which supports the campus-wide NMR shared resources that were utilized in this work. The authors are indebted to Nicholas J. Sherck for helpful suggestions and comments.

■ REFERENCES

(1) Makadia, H. K.; Siegel, S. J. Poly Lactic-co-Glycolic Acid (PLGA) as Biodegradable Controlled Drug Delivery Carrier. *Polymers* **2011**, *3*, 1377−1397.

(2) Hines, D. J.; Kaplan, D. L. Poly(lactic-co-glycolic) acid-controlled-release systems: experimental and modeling insights. *Crit. Rev. Ther. Drug Carrier Syst.* **2013**, *30*, 257−276.

(3) Zhong, H.; Chan, G.; Hu, Y.; Hu, H.; Ouyang, D. A Comprehensive Map of FDA-Approved Pharmaceutical Products. *Pharmaceutics* **2018**, *10*, 263.

(4) Wang, Y.; Qu, W.; Choi, S. H. FDA's regulatory science program for generic PLA/PLGA-based drug products. *Am. Pharm. Rev.* **2016**, *19*, 5−9.

(5) Tyler, B.; Gullotti, D.; Mangraviti, A.; Utsuki, T.; Brem, H. Polylactic acid (PLA) controlled delivery carriers for biomedical applications. *Adv. Drug Delivery Rev.* **2016**, *107*, 163−175.

(6) Lagreca, E.; Onesto, V.; Di Natale, C.; La Manna, S.; Netti, P. A.; Vecchione, R. Recent advances in the formulation of PLGA microparticles for controlled drug delivery. *Prog. Biomater.* **2020**, *9*, 153−174.

(7) Sharma, S.; Parmar, A.; Kori, S.; Sandhir, R. PLGA-based nanoparticles: a new paradigm in biomedical applications. *TrAC, Trends Anal. Chem.* **2016**, *80*, 30−40.

(8) Blasi, P. Poly(lactic acid)/poly(lactic-co-glycolic acid)-based microparticles: an overview. *J. Pharm. Invest.* **2019**, *49*, 337−346.

(9) Park, K.; Skidmore, S.; Hadar, J.; Garner, J.; Park, H.; Otte, A.; Soh, B. K.; Yoon, G.; Yu, D. J.; Yun, Y.; Lee, B. K.; Jiang, X. H.; Wang, Y. Injectable, long-acting PLGA formulations: Analyzing PLGA and understanding microparticle formation. *J. Controlled Release* **2019**, *304*, 125−134.

(10) Yun, Y. H.; Lee, B. K.; Park, K. Controlled Drug Delivery: Historical perspective for the next generation. *J. Controlled Release* **2015**, *219*, 2−7.

(11) Park, K.; Otte, A.; Sharifi, F.; Garner, J.; Skidmore, S.; Park, H.; Jhon, Y. K.; Qin, B.; Wang, Y. Formulation composition, manufacturing process, and characterization of poly(lactide-co-glycolide) microparticles. *J. Controlled Release* **2021**, *329*, 1150−1161.

(12) Gentile, P.; Chiono, V.; Carmagnola, I.; Hatton, P. V. An overview of poly(lactic-co-glycolic) acid (PLGA)-based biomaterials for bone tissue engineering. *Int. J. Mol. Sci.* **2014**, *15*, 3640−3659.

(13) Washington, M. A.; Balmert, S. C.; Fedorchak, M. V.; Little, S. R.; Watkins, S. C.; Meyer, T. Y. Monomer sequence in PLGA microparticles: Effects on acidic microclimates and in vivo inflammatory response. *Acta Biomater.* **2018**, *65*, 259−271.

(14) Stayshich, R. M.; Meyer, T. Y. New Insights into Poly(lactic-co-glycolic acid) Microstructure: Using Repeating Sequence Copolymers To Decipher Complex NMR and Thermal Behavior. *J. Am. Chem. Soc.* **2010**, *132*, 10920−10934.
(15) Li, J.; Stayshich, R. M.; Meyer, T. Y. Exploiting Sequence To Control the Hydrolysis Behavior of Biodegradable PLGA Copolymers. *J. Am. Chem. Soc.* **2011**, *133*, 6910−6913.
(16) Li, J.; Rothstein, S. N.; Little, S. R.; Edenborn, H. M.; Meyer, T. Y. The Effect of Monomer Order on the Hydrolysis of Biodegradable Poly(lactic-co-glycolic acid) Repeating Sequence Copolymers. *J. Am. Chem. Soc.* **2012**, *134*, 16352−16359.
(17) Stjerndahl, A.; Wistrand, A. F.; Albertsson, A.-C. Industrial utilization of tin-initiated resorbable polymers: synthesis on a large scale with a low amount of initiator residue. *Biomacromolecules* **2007**, *8*, 937−940.
(18) Barakat, I.; Dubois, P.; Jérôme, R.; Teyssié, P. Living polymerization and selective end functionalization of iε-caprolactone using zinc alkoxides as initiators. *Macromolecules* **1991**, *24*, 6542−6545.
(19) O'Keefe, B. J.; Hillmyer, M. A.; Tolman, W. B. Polymerization of lactide and related cyclic esters by discrete metal complexes. *J. Chem. Soc., Dalton Trans.* **2001**, 2215−2224.
(20) Hsiao, M.-W.; Wu, G.-S.; Huang, B.-H.; Lin, C.-C. Synthesis and characterization of calcium complexes: Efficient catalyst for ring-opening polymerization of L-lactide. *Inorg. Chem. Commun.* **2013**, *36*, 90−95.
(21) Lyubov, D. M.; Tolpygin, A. O.; Trifonov, A. A. Rare-earth metal complexes as catalysts for ring-opening polymerization of cyclic esters. *Coord. Chem. Rev.* **2019**, *392*, 83−145.
(22) Dutta, S.; Hung, W.-C.; Huang, B.-H.; Lin, C.-C. Recent Developments in Metal-Catalyzed Ring-Opening Polymerization of Lactides and Glycolides: Preparation of Polylactides, Polyglycolide, and Poly(lactide-co-glycolide). In *Synthetic Biodegradable Polymers*; Rieger, B.; Künkel, A.; Coates, G. W.; Reichardt, R.; Dinjus, E.; Zevaco, T. A., Eds.; Springer Berlin Heidelberg: Berlin, Heidelberg, 2012; pp 219−283.
(23) Li, X.-Q.; Wang, B.; Ji, H.; Li, Y. Insights into the mechanism for ring-opening polymerization of lactide catalyzed by Zn(C6F5)2/organic superbase Lewis pairs. *Catal. Sci. Technol.* **2016**, *6*, 7763−7772.
(24) Dechy-Cabaret, O.; Martin-Vaca, B.; Bourissou, D. Controlled Ring-Opening Polymerization of Lactide and Glycolide. *Chem. Rev.* **2004**, *104*, 6147−6176.
(25) Gilding, D. K.; Reed, A. M. Biodegradable polymers for use in surgery—polyglycolic/poly(actic acid) homo- and copolymers: 1. *Polymer* **1979**, *20*, 1459−1464.
(26) Skidmore, S.; Hadar, J.; Garner, J.; Park, H.; Park, K.; Wang, Y.; Jiang, X. Complex sameness: Separation of mixed poly(lactide-co-glycolide)s based on the lactide:glycolide ratio. *J. Controlled Release* **2019**, *300*, 174−184.
(27) Hadar, J.; Skidmore, S.; Garner, J.; Park, H.; Park, K.; Wang, Y.; Qin, B.; Jiang, X. Characterization of branched poly(lactide-co-glycolide) polymers used in injectable, long-acting formulations. *J. Controlled Release* **2019**, *304*, 75−89.
(28) Lohmeijer, B. G. G.; Pratt, R. C.; Leibfarth, F.; Logan, J. W.; Long, D. A.; Dove, A. P.; Nederberg, F.; Choi, J.; Wade, C.; Waymouth, R. M.; Hedrick, J. L. Guanidine and Amidine Organocatalysts for Ring-Opening Polymerization of Cyclic Esters. *Macromolecules* **2006**, *39*, 8574−8583.
(29) Ottou, W.; Sardon, H.; Mecerreyes, D.; Vignolle, J.; Taton, D. Update and challenges in organo-mediated polymerization reactions. *Prog. Polym. Sci.* **2016**, *56*, 64−115.
(30) Kiesewetter, M. K.; Scholten, M. D.; Kirn, N.; Weber, R. L.; Hedrick, J. L.; Waymouth, R. M. Cyclic Guanidine Organic Catalysts: What Is Magic About Triazabicyclodecene? *J. Org. Chem.* **2009**, *74*, 9490−9496.
(31) Kiesewetter, M. K.; Shin, E. J.; Hedrick, J. L.; Waymouth, R. M. Organocatalysis: Opportunities and Challenges for Polymer Synthesis. *Macromolecules* **2010**, *43*, 2093−2107.
(32) Zhang, X.; Jones, G. O.; Hedrick, J. L.; Waymouth, R. M. Fast and selective ring-opening polymerizations by alkoxides and thioureas. *Nat. Chem.* **2016**, *8*, 1047−1053.
(33) Yuan, H. Y.; Zhang, J. P. DBU-H (+) and H(2)o as effective catalyst form for 2,3-dihydropyrido 2,3-d pyrimidin-4(1H)-ones: A DFT Study. *J. Comput. Chem.* **2015**, *36*, 1295−1303.
(34) Brown, H. A.; De Crisci, A. G.; Hedrick, J. L.; Waymouth, R. M. Amidine-mediated zwitterionic polymerization of lactide. *ACS Macro Lett.* **2012**, *1*, 1113−1115.
(35) Kemo, V. M.; Schmidt, C.; Zhang, Y. F.; Beuermann, S. Low Temperature Ring-Opening Polymerization of Diglycolide Using Organocatalysts with PEG as Macroinitiator. *Macromol. Chem. Phys.* **2016**, *217*, 842−849.
(36) Jikei, M.; Suga, T.; Yamadoi, Y.; Matsumoto, K. Synthesis and properties of poly (L-lactide-co-glycolide)-b-Poly (ε-caprolactone) multiblock copolymers formed by self-polycondensation of diblock macromonomers. *Polym. J.* **2017**, *49*, 369−375.
(37) Sherck, N. J.; Kim, H. C.; Won, Y.-Y. Elucidating a unified mechanistic scheme for the DBU-catalyzed ring-opening polymerization of lactide to poly (lactic acid). *Macromolecules* **2016**, *49*, 4699−4713.
(38) Shieh, W.-C.; Dell, S.; Repic, O. Nucleophilic catalysis with 1, 8-diazabicyclo [5.4. 0] undec-7-ene (DBU) for the esterification of carboxylic acids with dimethyl carbonate. *J. Org. Chem.* **2002**, *67*, 2188−2191.
(39) Carafa, M.; Mesto, E.; Quaranta, E. DBU-Promoted Nucleophilic Activation of Carbonic Acid Diesters. *Eur. J. Org. Chem.* **2011**, *2011*, 2458−2465.
(40) Wang, R.; Luo, Y. W.; Li, B. G.; Zhu, S. P. Control of gradient copolymer composition in ATRP using semibatch feeding policy. *AIChE J.* **2007**, *53*, 174−186.
(41) Hamielec, A. E.; Macgregor, J. F.; Penlidis, A. MULTICOMPONENT FREE-RADICAL POLYMERIZATION IN BATCH, SEMIBATCH AND CONTINUOUS REACTORS. *Makromol. Chem., Macromol. Symp.* **1987**, *10−11*, 521−570.
(42) Qian, H.; Wohl, A. R.; Crow, J. T.; Macosko, C. W.; Hoye, T. R. A strategy for control of "random" copolymerization of lactide and glycolide: application to synthesis of PEG-b-PLGA block polymers having narrow dispersity. *Macromolecules* **2011**, *44*, 7132−7140.
(43) Dotson, N. A.; Galvan, R.; Laurence, R. L.; Tirrell, M. *Polymerization Process Modeling*; John Wiley & Sons, 1995.
(44) Klumperman, B. Mechanistic considerations on styrene−maleic anhydride copolymerization reactions. *Polym. Chem.* **2010**, *1*, 558−562.
(45) De Brouwer, H.; Schellekens, M. A.; Klumperman, B.; Monteiro, M. J.; German, A. L. Controlled radical copolymerization of styrene and maleic anhydride and the synthesis of novel polyolefin-based block copolymers by reversible addition−fragmentation chain-transfer (RAFT) polymerization. *J. Polym. Sci., Part A: Polym. Chem.* **2000**, *38*, 3596−3603.
(46) Hill, D.; Lang, A.; O'Donnell, J.; O'Sullivan, P. Determination of reactivity ratios from analysis of triad fractions—analysis of the copolymerization of styrene and acrylonitrile as evidence for the penultimate model. *Eur. Polym. J.* **1989**, *25*, 911−915.
(47) Kers, A.; Kers, I.; Stawinski, J. The reaction of diphenyl and dialkyl phosphorochloridates with 1,8-diazabicyclo 5.4.0 undec-7-ene (DBU). Formation of phosphonate diesters via N -> C phosphorus migration. *J. Chem. Soc., Perkin Trans. 2* **1999**, *10*, 2071−2075.
(48) Yu, Y. C.; Fischer, E. J.; Storti, G.; Morbidelli, M. Modeling of Molecular Weight Distribution in Ring-Opening Polymerization of L,L-Lactide. *Ind. Eng. Chem. Res.* **2014**, *53*, 7333−7342.
(49) Barton, A. F. M. *Handbook of Solubility Parameters and Other Cohesion Parameters*, 2nd ed.; CRC Press, 1991.
(50) Kravchenko, R.; Waymouth, R. M. Ethylene− propylene copolymerization with 2-arylindene zirconocenes. *Macromolecules* **1998**, *31*, 1−6.
(51) Liu, X.; Hua, X.; Cui, D. Copolymerization of lactide and cyclic carbonate via highly stereoselective catalysts to modulate copolymer sequences. *Macromolecules* **2018**, *51*, 930−937.

https://doi.org/10.1021/acs.iecr.1c03096
Ind. Eng. Chem. Res. 2021, 60, 14685−14700

(52) Beament, J.; Wolf, T.; Markwart, J. C.; Wurm, F. R.; Jones, M. D.; Buchard, A. Copolymerization of cyclic phosphonate and lactide: synthetic strategies toward control of amphiphilic microstructure. *Macromolecules* **2019**, *52*, 1220−1226.
(53) Scott, A. J.; Penlidis, A. Computational Package for Copolymerization Reactivity Ratio Estimation: Improved Access to the Error-in-Variables-Model. *Processes* **2018**, *6*, 8.
(54) Hauch, E.; Zhou, X. Q.; Duever, T. A.; Penlidis, A. Estimating Reactivity Ratios From Triad Fraction Data. *Macromol. Symp.* **2008**, *271*, 48−63.
(55) Agrawal, A.; Saran, A. D.; Rath, S. S.; Khanna, A. Constrained nonlinear optimization for solubility parameters of poly(lactic acid) and poly(glycolic acid)—validation and comparison. *Polymer* **2004**, *45*, 8603−8612.
(56) Brandup, J.; Immergut, E. H.; Grulke, E. A.; Abe, A.; Bloch, D. R. *Polymer Handbook*, 4th ed.; John Wiley & Sons: New York, 1999.
(57) Austin, A.-M. B.; Jacobson, S. Rate Matched Copolymerization. US Patent No. US2004/0266960A1, (Filed June 27, 2003), 2003.
(58) McGrath, J. E. Chain reaction polymerization. *J. Chem. Educ.* **1981**, *58*, 844−861.
(59) Ring, W.; Mita, I.; Jenkins, A.; Bikales, N. Source-based nomenclature for copolymers (Recommendations 1985). *Pure Appl. Chem.* **1985**, *57*, 1427−1440.
(60) Lutz, J. F. Defining the Field of Sequence-Controlled Polymers. *Macromol. Rapid Commun.* **2017**, *38*, No. 1700582.

https://doi.org/10.1021/acs.iecr.1c03096
Ind. Eng. Chem. Res. 2021, 60, 14685−14700